Chapter 15
Magnetocaloric Effect and Materials

J.R. Sun, B.G. Shen, and F.X. Hu

Abstract A brief review for magnetocaloric effect (MCE), including its potential application to magnetic refrigeration and the corresponding magnetic materials, has been given. Focuses are recent progresses in the exploration of magnetocaloric materials which exhibit a first-order phase transition, thus a giant MCE. Special issues such as proper approaches to determine the MCE associated with the first-order transition and the effects of lattice and electronic entropies are discussed. The applicability of the giant MCE materials to the magnetic refrigeration near ambient temperature is evaluated.

15.1 Introduction

Magnetic materials can absorb or expel heat in magnetizing or demagnetizing process. This phenomenon is called magnetocaloric effect (MCE). When magnetized, magnetic moments of the materials tend to aligning in parallel. This causes a decrease of magnetic entropy (ΔS), thus a heat release (amounted to $T|\Delta S|$) to environment, where T is temperature. On the contrary, the arrangement of magnetic moments becomes disordered after removing magnetic field. Corresponding to the increase of magnetic entropy, heat from the surroundings has to be absorbed to keep the materials at a constant temperature. The former causes an increase, whereas the latter a decrease of environment temperature. This is the principle based on which magnetic refrigerator works. The MCE of the materials is characterized by two important quantities. The first one is the field-induced isothermal entropy change ΔS and the second one the adiabatic temperature change ΔT_{ad}. There is an approximate relation between ΔS and ΔT_{ad}: $\Delta T_{ad} \approx T\Delta S/C$, where C is the heat capacity of the materials.

J.R. Sun (✉)
State Key Laboratory for Magnetism, Institute of Physics, Chinese Academy of Sciences, Beijing 100080, Peoples' Republic of China
e-mail: jrsun@g203.iphy.ac.cn

J.P. Liu et al. (eds.), *Nanoscale Magnetic Materials and Applications*,
DOI 10.1007/978-0-387-85600-1_15,

In addition to the potential application to magnetic refrigeration, the MCE is also fundamentally important for the study of magnetism. It can provide valuable information, which may be unavailable for other techniques, about magnetic transition. It also has a strong impact on physical arguments such as entropy, specific heat, and thermal conduction, etc.

The MCE was first discovered by Warburg in 1881 when studying the magnetic behaviors of Iron [1]. Langevin gave the first theoretical explanation [2]. He found that reversible temperature change generally occurred when the magnetization (M) of a paramagnetic (PM) system altered under applied field. The ones who first foresaw the technological potential of this effect is Debye and Giauque [3, 4]. They pointed out, independently, that ultra-low temperatures could be reached through the reversible temperature change of PM salts with the alternation of magnetic field. The first experiment of magnetic refrigeration was performed in 1933, by Giauque and MacDougall [5]. With the use of this technology, the temperatures below 1 K were successfully gained, which won Giauque the Nobel Prize of 1949. Subsequent work proved that, via adiabatic demagnetizing of nuclear magnetism, ultra-low temperatures in nanokelvin range can be reached [6]. Nowadays, magnetic refrigeration has become one of the basic technologies getting ultra-low temperatures.

In contrast to the success in the ultra-low temperature range, the application of this technique in lifted temperature ranges such as 1.5−20 K, the range for liquid helium, and 20−80 K, the range for liquid hydrogen and liquid nitrogen, is relatively limited. The mature refrigerants for the range from 1.5 to 20 K are the garnets of the formula $R_3M_5O_{12}$ (R = Nd, Gd, and Dy; M=Ga and Al), $Gd_2(SO_4)_3.8H_2O$ [7], $Dy_3Al_5O_{12}$ (DAG) [8]. The most typical material is $Gd_3Ga_5O_{12}$ (GGG), which has been successfully used to the precooling for the preparation of liquid helium. As for the temperature range 20−80 K, the modest refrigerants are Nd, Er, Tm, and RAl_2 (R = Er, Ho, Dy, $Dy_{0.5}Ho_{0.5}$, Dy_xEr_{1-x}, and GdPd), RNi_2(R = Gd, Dy, and Ho). The RAl_2-type compounds have obvious advantages over others because of its broad phase transition. For example, $(ErAl_{2.15})_{0.312}(HoAl_{2.15})_{0.198}(Ho_{0.5}Dy_{0.5}Al_{2.15})_{0.49}$ has the curie temperature between 10 and 40 K [9] and $(ErAl_{2.2})_{0.3055}$:$(HoAl_{2.2})_{0.1533}(Ho_{0.5}Dy_{0.5}Al_{2.2})_{0.252}$ between 15 and 77 K [10]. A detailed review of the magnetic refrigeration technology and corresponding materials in these temperature ranges has been given by Tishin and Spichkin [11] and will not be repeated here.

Magnetic refrigeration near room temperature is of special interest because of its great social effect and economical benefit. Compared with the technology based on the gas compression/expansion, which is widely used today, magnetic refrigeration is environment friendship and energy saving. It is also a silent cooling technique because of the absence of compressor. The great challenge to room-temperature magnetic refrigeration, in addition to the improvement of refrigerator apparatus, is the lacking of effective refrigerants. Due to the significant increase of heat capacity near the ambient temperature, the heat transferred by each magnetizing–demagnetizing cycling of the refrigerator should be considerably large to guarantee refrigeration efficiency. As a result, most of the materials working at low temperatures cannot be directly utilized, and new materials with great entropy change around the ambient temperature must be explored.

The first milestone in the long march to room-temperature refrigeration is the work of Brown in 1976 [12], which showed that Gd is a reasonable working material near room temperature. Based on this result, Zimm and his colleagues designed the first proof-of-principle magnetic refrigerator in 1998 [13]. This machine worked for 18 months with a coefficient of performance (COP) of 15 and a maximal cooling power of 600 W over a temperature span of 10 K for the field change of 0−5 T. This is the first demonstration that magnetic refrigeration is a competitive cooling technology near room-temperature region. Another important breakthrough is the discovery of giant MCE by Gschneidner and his colleagues in 1997 [14, 15]. It was found that the entropy change of $Gd_5Si_2Ge_2$, for a field variation of 0−5 T, is ∼18 J/kgK around 280 K, significantly larger than that of Gd (∼10 J/kgK) under similar conditions. New materials such as $LaFe_{13-x}Si_x$ [16, 17], $MnAs_{1-x}Sb_x$($0<x<0.3$) [18], and $MnFeP_{0.45}As_{0.55}$ [19] were subsequently reported showing the entropy changes from 18 to 30 J/kgK near the ambient temperature. These achievements stimulated a new wave of MCE research.

A common feature of the giant MCE is that it usually occurs accompanying a first-order magnetic transition. The sharp phase transition and its shift under applied field confine ΔS to a narrow temperature range, which is the apparent reason for the enhancement of MCE. However, several basic problems involved in the MCE arising from the first-order phase transition must be solved. For example, the determination of MCE, the contributions other than magnetic entropy to MCE, and the effects of magnetic/thermal hysteresis as far as practical application being concerned. In this article, we will give first a brief discussion about these problems, then a review for the typical magnetic materials with giant MCE. Special attention has been paid to recent progresses in the MCE researches.

15.2 Theoretical Description of Magnetocaloric Effect

In this section, the general description of the MCE will be discussed. Based on the standard thermodynamics, the differential free energy of a system under magnetic field H, pressure P, and at temperature T will be $dG=VdP-SdT-MdH$. The entropy of the system has the form

$$S(T, H, P) = -\left(\frac{\partial G}{\partial T}\right)_{H,P}, \tag{15.1}$$

and the magnetization the form

$$M(T, H, P) = -\left(\frac{\partial G}{\partial H}\right)_{T,P}. \tag{15.2}$$

Based on Eqs. (15.1) and (15.2), the well-known Maxwell relations can be obtained,

$$\left(\frac{\partial S}{\partial H}\right)_{T,P} = \left(\frac{\partial M}{\partial T}\right)_{H,P} \tag{15.3}$$

In the case of fixed pressure and temperature, we have the following equation:

$$dS = \left(\frac{\partial M}{\partial T}\right)_{H,P} dH. \tag{15.4}$$

The isothermal entropy change can be obtained by integrating Eq. (15.4),

$$\Delta S\,(T,\,H,\,P) = S\,(T,\,H,\,P) - S\,(T,\,H=0,\,P) = \int_0^H \left(\frac{\partial M}{\partial T}\right)_{H,P} dH \tag{15.5}$$

In general, the entropy change induced by external field is calculated by Eq. (15.5) based on magnetic data $M(T, H)$. In practice, the following formula is also used

$$\Delta S\,(T,\,H,\,P) = \int_0^T \frac{\left(C_{H,P} - C_{0,P}\right)}{T} dT \tag{15.6}$$

where $C_{\mathrm{H,P}}$ and $C_{\mathrm{0,P}}$ are the heat capacities in the fields of H and 0, respectively, under a constant pressure of P.

For a simple PM system or a ferromagnetic (FM) system above Curie temperature, $M = C_{\mathrm{J}}H/T$ or $CH/(T{-}T_{\mathrm{C}})$, where $C_J = N\mu_B^2 g_J^2\, J(J+1)$ is the Curie–Weiss constant. The corresponding magnetic entropy change is $\Delta S = -C_{\mathrm{J}}\Delta H^2/2T^2$ or $-C_{\mathrm{J}}\Delta H^2/2(T{-}T_{\mathrm{C}})^2$.

In fact, the entropy of a magnetic material is composed of magnetic entropy S_{M}, electronic entropy S_{E}, and lattice entropy S_{L}. The magnetic entropy of the spin system is determined by the free energy of the magnetic sublattice, and it has the form

$$S_M(T,\,H) = Nk_B\left[\ln\frac{\sinh(\frac{2J+1}{2J}x)}{\sinh(\frac{1}{2J}x)} - xB_J(x)\right] \tag{15.7}$$

within the mean-field approximation, where $\mathrm{x}{=}gJ\mu_{\mathrm{B}}H/k_{\mathrm{B}}T$, with J being the quantum number of angular momentum, k_{B} the Boltzmann constant, g the Lander factor, and B_{J} the Brillouin function. In the high temperature and low-field limit ($\mathrm{x}{<<}1$), we have

$$S_M = Nk_B\left[\ln(2\,J+1) - \frac{1}{2}\frac{C_J H^2}{(T-T_C)^2}\right] \tag{15.8}$$

For a complete order–disorder transition, the magnetic entropy will get its maximal value of $S_M = Nk_B\ln(2\,J+1)$.

The electronic entropy has the form of $S_E = \gamma T$, where γ is the coefficient of electronic heat capacity. Contribution from electronic entropy can be ignored at high temperatures. Based on the Debye approximation, entropy associated with phonon can be expressed as

$$S_L = R\left[-3\ln(1-e^{\theta_D/T}) + 12\left(\frac{T}{\theta_D}\right)^3 \int_0^{\theta_D/T} \frac{x^3 dx}{e^x - 1}\right] \tag{15.9}$$

where R is the gas constant, and θ_D the Debye temperature. In the case of $T > \theta_D$, a direct estimation indicates that the higher the θ_D is, the smaller the lattice entropy will be. For a first-order transition, contributions of electronic and lattice entropy, which is negligible for a second-order one, cannot be simply ignored due to the discontinuous change of order parameter at T_C.

After a simple derivation, the adiabatic temperature change ΔT_{ad}, upon the variation of external field, can also be obtained. According to the standard thermodynamics, the differential entropy has the form,

$$dS = \left(\frac{\partial S}{\partial T}\right)_{H,P} dT + \left(\frac{\partial S}{\partial H}\right)_{T,P} dH + \left(\frac{\partial S}{\partial P}\right)_{T,H} dP \tag{15.10}$$

$dS = 0$ under the adiabatic condition, then the adiabatic temperature change will be,

$$dT = -\frac{T}{C_{H,P}}\left(\frac{\partial M}{\partial T}\right)_{H,P} dH, \tag{15.11}$$

where $C_{H,P}$=$T(\partial S/\partial T)_{H,P}$ denotes heat capacity. Integrating Eq. (15.11) over $H = 0$-H, we get the adiabatic temperature change. Therefore, to obtain ΔT_{ad}, both the magnetic data $M(H,T)$ and the heat capacity are required. As will be discussed later, this is an indirect technique for the determination of ΔT_{ad}.

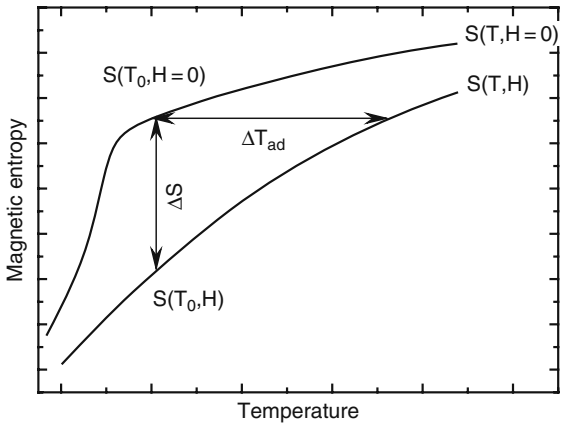

Fig. 15.1 A schematic for the entropies under the fields of 0 and H, respectively. The *horizontal arrow* marks adiabatic temperature change, and the *vertical* one marks the entropy change as magnetic field increases

There is a simple relation between ΔS and ΔT_{ad} as shown by the schematic in Fig. 15.1, which illustrates the entropies under the field of 0 and H, respectively. In the case of increasing magnetic field while keeping temperature constant, the entropy change will be the perpendicular distance of the two curves at T_0. However, if there is no heat exchange between magnetic material and its surroundings, that is,

$\Delta S = 0$, the application of a magnetic field will cause an increase in temperature (ΔT_{ad}) of the magnetic materials.

15.3 Experimental Determination of Magnetocaloric Effect

The two quantities ΔT_{ad} and ΔS that characterize the MCE of magnetic materials can be determined either directly or indirectly [20].

15.3.1 Direct Measurement of Adiabatic Temperature Change

Without heat exchange with surroundings, temperature of the magnetic materials will suffer from a detectable change while an external field is applied as schematically shown in Fig. 15.1. If the initial temperature of the sample is T_i and the final temperature T_f corresponding to the field increase from 0 to H, the adiabatic temperature change will be $\Delta T_{ad} = T_f(H) - T_i(0)$.

The adiabatic property of the measuring unit where the sample is settled, the thermal contact between the sample and the temperature sensors, the sensitivity of temperature sensors, influence of external field on temperature sensor, and thermal or magnetic hysteresis of the materials are crucial factors affecting the accuracy of the measurement. The detected ΔT_{ad} is generally smaller than the real value, with an error about 10%.

To minimize the effect of thermal leakage, a field change as rapid as possible is desired for the direct measurement of ΔT_{ad}. It is not easy to realize a rapid field change, especially for the superconducting magnet. As an alternative, the sample is usually moved rapidly into or out of the magnetic field. In the past 80 years, much effort has been devoted to the improvement of experiment accuracy, and various technologies have been developed. A detailed description can be found in the monograph of Tishin and Spichkin [11].

15.3.2 Indirect Measurement of Entropy and Adiabatic Temperature Changes

Direct measurement gives only the information about adiabatic temperature change. To determine isothermal magnetic entropy change, two important indirect methods have to be invoked. The first one is the estimation of ΔS by Eq. (15.5) using the magnetization isotherms collected under different temperatures in the interested region. In reality, an alternative formula, equivalent to Eq. (15.5), is usually used for numerical calculation,

$$\Delta S = \sum_i \frac{M_{i+1} - M_i}{T_{i+1} - T_i} \Delta H_i, \tag{15.12}$$

where M_i and M_{i+1} are the magnetizations at the temperatures T_i and T_{i+1}, respectively. This is the most frequently used approach for the determination of ΔS because of its effectiveness, efficiency, and convenience. The accuracy of the ΔS values thus obtained is influenced by the uncertainty of magnetic moment, temperature, and magnetic field, and the errors are estimated to be 3−10%.

Alternatively, ΔS can also be estimated from the heat capacity data. According to the thermodynamics, there is a relation between entropy and heat capacity

$$S(T, H) = \int_0^T \frac{C(T, H)}{T} dT, \tag{15.13}$$

where the constant pressure P has been omitted. Two $S-T$ relations $S(T, H=0)$ and $S(T, H)$ can be obtained based on Eq. (15.13) using the data collected under corresponding fields, which lead to the isothermal entropy change of the form: $\Delta S(T, H)=S(T, H)-S(T, H=0)$. Noting the one-to-one correspondence between S and T, a $T(S, H)$ relation can be derived from $S(T, H)$. This in turn gives the adiabatic temperature change: $\Delta T_{ad}(T, H) = T(S, H)-T(S, 0)$.

The accuracy of the ΔS and ΔT_{ad} values thus obtained depends on the precision of heat capacity, and the errors are generally the order of 10%, varying with temperature. Pecharsky and Gschneidner have given a systematic analysis about the uncertainty of the entropy and adiabatic temperature changes experimentally determined [20].

15.4 Magnetocaloric Effect Associated with First-Order Phase Transition

It should be noted that Eq. (15.5) is derived for the second-order phase transition. Because of the discontinuous change of M at T_C for the first-order magnetic transition, it is a problem whether the Maxwell relation can be utilized to determine entropy changes. Two different cases, an idealized and a non-idealized first-order phase transitions, should be considered.

15.4.1 MCE Due to an Idealized First-Order Phase Transition

In this case, Eq. (15.12) can still be used to calculate ΔS. For an idealized first-order transition, that is, the magnetization is a step function of temperature, Sun et al. [21] showed that the Maxwell relation and the Clausius–Clapeyron equation gave similar results. Based on the integrated Maxwell relation, entropy change can be expressed as

$$\Delta S(T) = \int_0^H \left(\frac{\partial M}{\partial T}\right)_{H,P} dH = \int_{T_C(0)}^{T_C(H)} \Delta M \delta(T - T_C) \left(\frac{dT_C}{dH}\right)_{H,P}^{-1} dT_C = \frac{\Delta H \Delta M}{\Delta T_C}, \tag{15.14}$$

where the equalities $(\partial M/\partial T)_{H,P} = -\Delta M\delta(T-T_C)$ and $dT_C/dH = \Delta T_C/\Delta H$ have been used. The right side of Eq. (15.14) is exactly the entropy change predicted by the Clausius–Clapeyron equation. It reveals a constant entropy change in the temperature range between $T_C(0)$ and $T_C(H)$ whereas null otherwise, without the effects from the variation of magnetic order parameter. This work proves the applicability of the Maxwell relation to first-order phase transition.

15.4.2 MCE Due to a Non-Idealized First-Order Phase Transition

15.4.2.1 In the Vicinity of Curie Temperature

In reality, a first-order phase transition occurs in a finite temperature range, and two phases coexist in the transition process. Liu et al. [22] found that in this case the Maxwell relation can yield a spurious ΔS peak in the vicinity of the Curie temperature $T_C(H = 0)$.

A typical example is the cubic $NaZn_{13}$-type intermetallic $La_{0.7}Pr_{0.3}Fe_{11.5}Si_{1.5}$. Figure 15.2 shows the magnetization isotherms of $La_{0.7}Pr_{0.3}Fe_{11.5}Si_{1.5}$ measured in the field ascending process. The compound is completely FM below 183 K and PM above 185 K without external field. A stepwise magnetic behavior appears at the temperature of 184 K, signifying the coexistence of FM and PM phases. The first steep increase of magnetization marks the contribution of the FM phase, while the subsequent stair-like variation signifies the filed-induced FM transition of the PM phase.

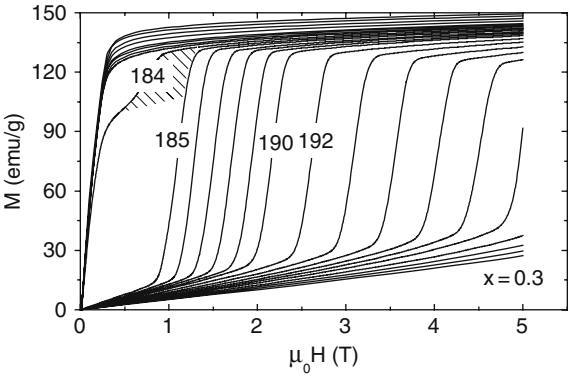

Fig. 15.2 Magnetization isotherms of $La_{0.7}Pr_{0.3}Fe_{11.5}Si_{1.5}$ measured by ascending magnetic field. *Hatched area* marks the area that contributes to entropy change. Numbers in the figure denote the temperature in the units of Kelvin (Ref. [22])

The corresponding entropy change calculated by the Maxwell relation is shown in Fig. 15.3 ($\Delta H = 5$ T). In addition to the flat ΔS plateau of the height of ~28 J/kg K, an extra spike-shaped peak of the height of ~99.6 J/kgK appears at exactly the same temperature where stepwise magnetic behaviors appear. The heat capacity of this compound was also measured under the fields of 0 and 5 T, and the entropy change calculated by Eq. (15.13) indicates the absence of the spike ΔS

peak. These results show the failure of the Maxwell relation, which cannot give a correct result for the entropy change near T_C.

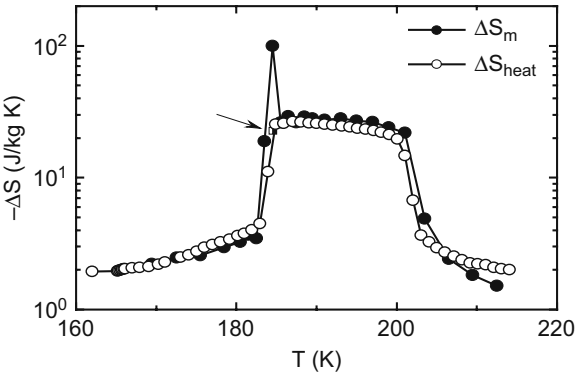

Fig. 15.3 Temperature-dependent entropy changes of $La_{0.7}Pr_{0.3}Fe_{11.5}Si_{1.5}$ calculated from magnetic data (*solid circles*) and heat capacity (*open circles*), respectively (Ref. [22])

Considering the fact that magnetic field affects only the magnetic state of PM phase, which coexists with the FM phase near T_C, only the PM phase contributes to thermal effect. With this in mind, a modified equation for the calculation of ΔS can be established. Figure 15.4 is a schematic showing the determination of ΔS for the system with an idealized stepwise behavior. Denoting the area surrounded by the two $M-H$ curves at T_1 and T_2 as $\Sigma_1+\Sigma_2$, the Maxwell relation gives $\Delta S = (\Sigma_1+\Sigma_2)/(T_1-T_2)$. Considering the fact that the field-induced meta-magnetic transition takes place in the PM phase, only Σ_1 contributes to ΔS. This implies $\Delta S = \Sigma_1/(T_1-T_2)$.

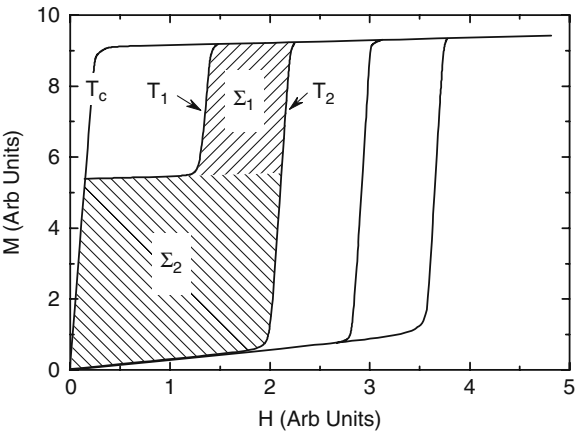

Fig. 15.4 A schematic showing the calculation of entropy change when stepwise magnetic behaviors occur (Ref. [22])

Stepwise magnetic behaviors widely exist in magnetic materials such as $MnAs_{1-x}Fe_x$ [23] and $Gd_5Si_{4-x}Ge_x$ [24]. It was also observed in MnAs [25] and $Mn_{1-x}Cu_xAs$ [26] under high pressures. It could be a general feature of the first-order phase transition because the finite temperature width of the phase transition. In this case, ΔS should be handled carefully.

15.4.2.2 MCE Associated with Complex Magnetic Phase Transitions

When more than two phases coexist in a wide temperature range, applicability of the Maxwell relation should also be checked carefully considering the fact that this relation is derived for a homogeneous system in the equilibrium state. Liu et al. [27] found that if the proportions of the coexisted phases change with either magnetic field or temperature, the Maxwell relation may predict incorrect results.

A typical example is manganite $Eu_{0.55}Sr_{0.45}MnO_3$. It exhibits a complex magnetic behavior. As shown in Figure 15.5, two magnetic processes take place sequentially on cooling under a field between 0.5 and 2 T. The first one is a PM to FM transition, while the second one is a FM to antiferromagnetic (AFM) transition. In the intermediate, temperature and magnetic field range FM and AFM/PM phases coexist. The fully FM polarized state is obtained above ~2.3 T.

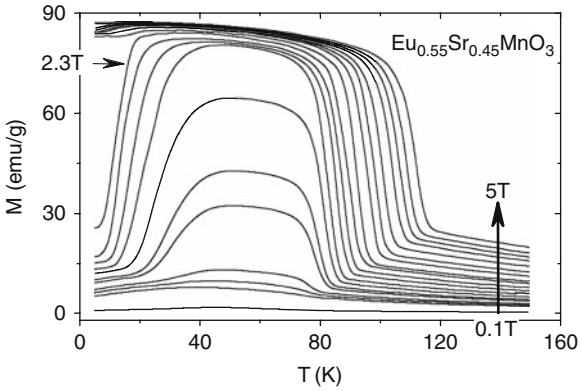

Fig. 15.5 Thermal magnetization of $Eu_{0.55}Sr_{0.45}MnO_3$ measured under different magnetic fields

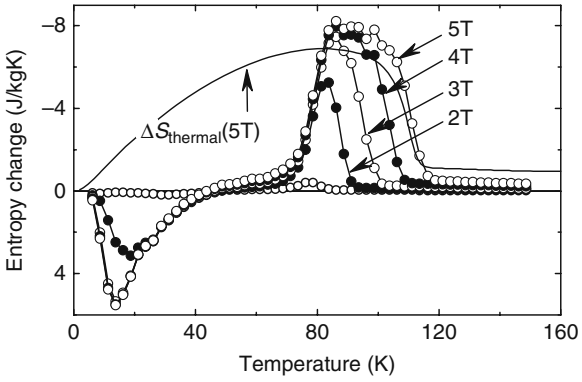

Fig. 15.6 Entropy changes in $Eu_{0.55}Sr_{0.45}MnO_3$ determined by Maxwell relation (*symbols*) and specific heat (*solid line*)

Figure 15.6 exemplifies the entropy changes calculated by Eqs. (15.12) and (15.6), based on magnetization isotherms and heat capacity data, respectively. The most striking observation is the significant discrepancy between the two results.

Different from the entropy increase below ~40 K predicted by the Maxwell relation, the calorimetric measurement declares an entropy decrease in the whole temperature range below ~110 K. Similar results are also observed in other compounds such as $La_{0.27}Nd_{0.40}Ca_{0.33}MnO_3$, etc. [27].

According to the standard thermodynamics theory, when two phases coexist the entropy change will be

$$\Delta S = X_0 \Delta S_2 + \int_0^T \left(\Delta X_1 C_{p1} - \Delta X_1 C_{p2}\right) dT/T \tag{15.15}$$

where X_0 is the total volume, and X_1 the volume occupied by FM phase, C_{p1} and C_{p2} are the heat capacities (per volume) of the FM and non-FM phases, respectively. $\Delta S_2 = S_2(T,H)\text{-}S_2(T,0)$ and $\Delta X_1 C_p = X_1(T,H)C_p(T,H)\text{-}X_1(T,0)C_p(T,0)$ (S_2 the entropy of non-FM phase). In contrast, the Maxwell relation gives

$$\begin{aligned}\Delta S = {} & X_0 \Delta S_2 + \int_0^T \left(\Delta X_1 C_{p1} - \Delta X_1 C_{p2}\right) dT/T \\ & + \int_0^H (M_1 - M_2)\left(\partial X_1/\partial T\right)_H dH \\ & - \int_0^T dT/T \int_0^H \left(C_{p1} - C_{p2}\right)\left(\partial x_1/\partial H\right)_T dH\end{aligned} \tag{15.16}$$

where the relation $M = X_0 M_2 + X_1(M_1 - M_2)$ has been used. It is obvious that the same results are obtained only when X_1 is independent of T and H. In most of the phase-separated compounds, the filed-induced FM transition does not occur until a threshold field is reached. Below this field, the Maxwell relation can still be used based on the above arguments. However, when the applied field is so large as to affect the proportion of the FM or non-FM phase in the compound, calorimetric data have to be used.

15.5 Typical Materials with Giant Magnetocaloric Effect

Since the success of the magnetic refrigeration at ultra-low temperatures, the attempt to apply this technology to higher temperatures has never stopped. Because of the increase of heat capacity, the materials working in the low-temperature region cannot be directly used at high temperatures. To get effective MCE materials becomes one of the key problems to be solved. The discovery of new magnetic materials with giant MCE in the last decade, together with the successful demonstration of the proof-of-principle refrigerators working near the ambient temperature, displays a bright prospect of magnetic cooling.

There are three categories of magnetocaloric materials as classified by the temperature where the maximal MCE occurs: the low-temperature materials (below 20 K), the materials for intermediate temperatures (20−80 K), and the materials

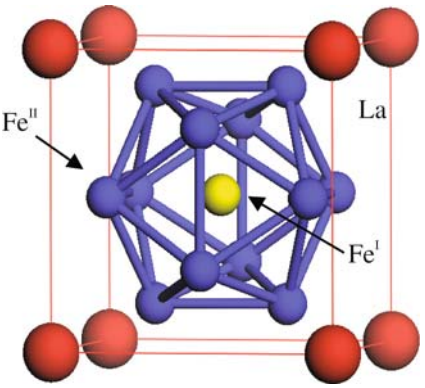

Fig. 15.7 A schematic of the atomic structure of $LaFe_{13}$

for the temperatures above 80 K. A detailed description for the first two kinds of materials can be found elsewhere [11, 28]. In the following, we will focus our attention on the recently discovered high-temperature MCE materials.

15.5.1 $LaFe_{3-x}M_x$ (M = Al, Si) Intermetallics

The cubic $NaZn_{13}$-type intermetallics $LaFe_{13-x}M_x$ (M=Si and Al) have attracted great attention due to their giant MCE, small hysteresis loss, and high thermal conductivity and have been regarded as one of the most promising candidates for magnetic refrigerants.

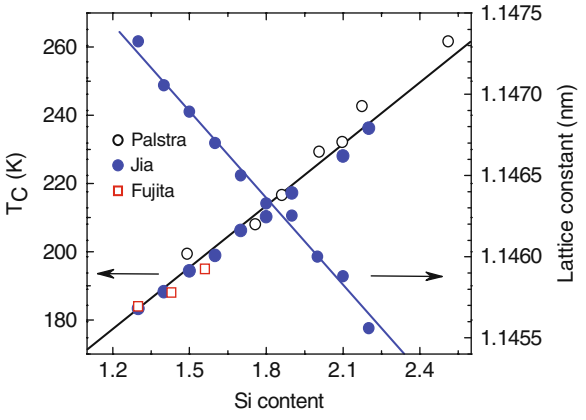

Fig. 15.8 Curie temperature and lattice constant as functions of Si content for $LaFe_{13-x}Si_x$. Data were obtained from Refs. [32] (Palstra), [38] (Jia), and [39] (Fujita)

15.5.1.1 Generic Magnetic Properties

$LaCo_{13}$ is the only stable $NaZn_{13}$-type La-transition-metal intermetallic showing a Curie temperature of ~1,318 K [29]. Different from $LaCo_{13}$, $LaFe_{13}$ is unstable due to its positive formation enthalpy, and minor additions such as Si and/or Al are required to stabilize the structure [30]. Figure 15.7 is the fictitious structure of $LaFe_{13}$. The crystal structure is cubic, and the space group is Fm3c. Fe atoms occupy two different crystallographic sites of 8b (Fe^{I}) and 96I (F^{II}) at a ratio of 1:12. Eight $LaFe_{13}$ clusters are contained in each unit cell. La and Fe^{I} form the CsCl structure, and each La is surrounded by 24 Fe^{II} atoms. Fe^{I} situates at the center of the icosahedron formed by 12 Fe^{II} atoms.

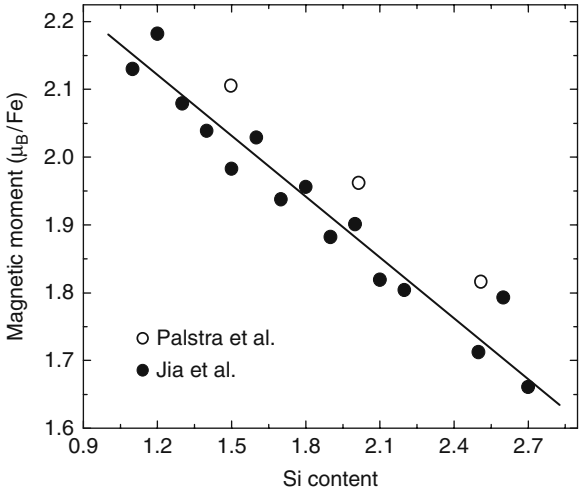

Fig. 15.9 Magnetic moment of Fe atoms in $LaFe_{1-x}Si_x$. Data were obtained from Refs. [32] (Palstra) and [38] (Jia)

The $LaFe_{13-x}M_x$ compounds were first successfully synthesized by Kripyakevich et al. in 1968 [30]. With the incorporation of Al or Si, the lattice parameter increases or decreases linearly. The magnetic properties of $LaFe_{13-x}M_x$ were investigated by Palstra et al. [31, 32], Heimhold et al. [33], Tang et al. [34], Fujita and Fukamichi [35], Fujita et al. [36], and Hu et al. [37]. These studies showed that $LaFe_{13-x}Si_x$ is PM near the ambient temperature and undergoes a FM transition upon cooling at a temperature between 200 and 250 K (depending on Si content). Palstra et al. found that T_C increased linearly from ~199 K for x=1.5 to ~261 K for x=2.5. These results were confirmed by the subsequent work by Jia et al. [38] and Fujita et al. [39] (Fig. 15.8). Palstra et al. [32] and Jia et al. [38] also observed a monotonic decrease of saturation magnetization, at a rate of $-0.286\ \mu_B$ for each Si, with the increase of Si content (Fig. 15.9). This means that the decrease of saturation magnetization is not a simple dilution effect of Fe by Si. A first-principle calculation conducted by Wang et al. [40] indicated the occurrence of hybridization between the Fe-3d and the Si-2p electrons and the change of the density of state below Fermi surface after the introduction of Si, which could be the reason for the change of Fe magnetic moment.

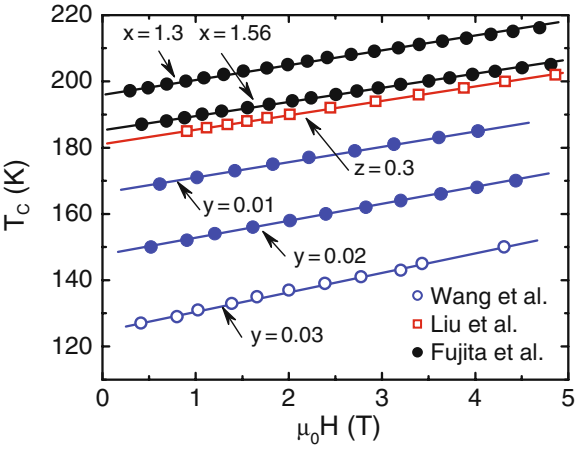

Fig. 15.10 Curie temperature as a function of magnetic field for the compounds $LaFe_{13-x}Si_x$ (Ref. [39]), $La(Fe_{1-y}Mn_y)Si_{1.3}$ (Ref. [41]), and $La_{1-z}Pr_zFe_{11.5}Si_{1.5}$ (Ref. [21])

The magnetic transition was found to be first order when x is small for M=Fe, manifested by the steep drop of magnetization across T_C and the occurrence of considerable thermal or magnetic hysteresis. An evolution of the phase transition from first order to second order takes place as x increases, and a typical second-order transition appears when $x > 1.8$.

Magnetic field can drive T_C of the first-order transition to high temperatures at a rate of ~4.3 K/T. This is an effect essentially independent of the composition of the compounds. Figure 15.10 displays the field-dependent Curie temperature for the compounds of $LaFe_{13-x}Si_x$, $La_{1-z}Pr_zFe_{11.5}Si_{1.5}$, and $LaFe_{11.7-y}Mn_ySi_{1.3}$, based on data obtained by Wang et al. [41], Liu et al. [22] and Fujita et al. [39] respectively. These results indicate that magnetic field affects the $LaFe_{13}$-based compounds in essentially the same way, regardless of composition.

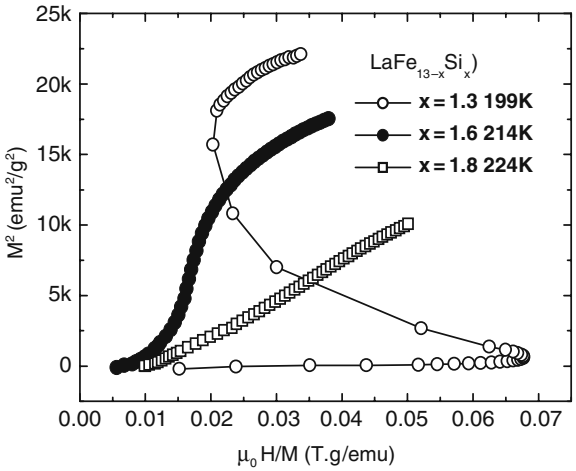

Fig. 15.11 Arrott plots of $LaFe_{1-x}Si_x$ at the temperature just above T_C

The high-temperature shift of T_C under applied field implies the occurrence of field-induced meta-magnetic transition of the PM phase, an itinerant-electron meta-magnetic (IEM) transition as claimed by Fujita et al. [36]. The FM state becomes more stable than the PM state under applied field due to the field-induced change in the band structure of 3d electrons. The IEM transition is usually marked by the appearance of "S"-shaped M^2-H/M isotherms (Arrott plot). For the $LaFe_{13}$-based compounds, the lower the Si content is, the stronger the first-order nature of the magnetic transition will be (Fig. 15.11).

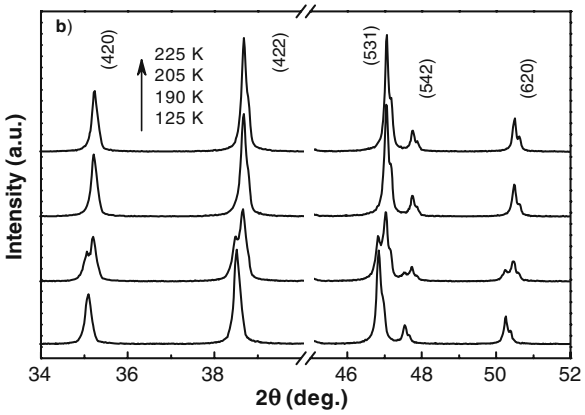

Fig. 15.12 X-ray diffraction spectra of $LaFe_{13-x}Si_x$ for $x = 1.2$ collected under different temperatures. The peak splitting at the temperature of 190 K is a result of two-phase coexistence (Ref. [37])

The lowest Si content in the previously studied compound is x=1.5. Hu et al. [37] successfully extended x to lower values by vacuum annealing the as-prepared samples at a temperature as high as ~1,150°C for more than 30 days and found that the lowest Si content required for the stabilization of the compound is x~1.2. Figure 15.12 shows the powder X-ray diffraction spectra of $LaFe_{13-x}Si_x$ with x=1.2 collected under different temperatures. No secondary phase is detected. Insufficient annealing will lead to the presence of α-Fe.

When the content of Si is high, the structure of $LaFe_{13-x}Si_x$ becomes tetragonal of the $Ce_2Ni_{17}Si_9$-type as reported by Tang et al. [34]. Ferromagnetism remains for $2.6 < x < 3$, while vanishes when $3 < x < 5$.

The introduction of Al, instead of Si, can also stabilize $LaFe_{13}$-type intermetallics [32]. Different from Si doping, however, the incorporation of Al leads to complex magnetic behaviors. The compound is paramagnetic at high temperatures, regardless of Al content. In the low-temperature range, in contrast, it is micromagnetic for $0.4 < x < 0.6$, FM for x 0.7 $< x < 1.04$, and antiferromagnetic for $1.04 < x < 1.82$. It is interesting that partial replacement of Fe by Co can completely depress the AFM state. Hu et al. [42] found that $La(Fe_{1-y}Co_y)_{13-x}Al_x$ (x=1.3) becomes FM when minor Co atoms (y=0.02) are introduced. This result reveals the small difference between the free energies of the AFM and the FM states.

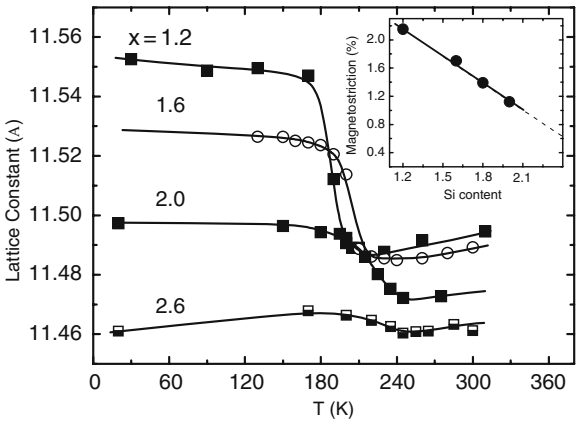

Fig. 15.13 Lattice constant as a function of temperature of $LaFe_{13-x}Si_x$ (Ref. [44])

15.5.1.2 Spontaneous Magnetostriction of $LaFe_{13-x}Si_x$

The lattice constant of $LaFe_{13-x}Si_x$ with a Si content below x=1.8 is weakly temperature dependent, decreasing slightly as temperature increases. Accompanying the PM to FM transition, a significant, yet sharp, change in phase volume takes place, especially when the Si content is low. The relative volume change at T_C is ~1.2% for x=2 and ~2.1% for x=1.2, as shown in Fig. 15.13. Wang et al. [43] proved that the peculiar temperature dependence of the lattice constant is a combined effect of spontaneous magnetostriction and thermal expansion. For the $LaFe_{13-x}Si_x$ compounds, the spontaneous magnetostriciton is particularly obvious. Based on the analysis of neutron diffraction data, Wang et al. [43] established a quantitative relation $(\Delta V/V - 3\gamma T) = 0.018\sigma^2$ for the sample $LaFe_{13-x}Si_x$ (x=1.6), where $\Delta V/V$ is the relative volume change, σ the normalized magnetization, and γ the linear thermal expansivity. It means a maximum magnetostriction of ~1.8%, quite similar to that of FeNi-invar alloy (1.9%). The result of Wang et al. was obtained in the temperature range below T_C. By comparing the $\Delta V/V - T$ (obtained from the X-ray diffraction analyses) and the σ-T dependences in a wide temperature range below 300 K, alternatively, Jia et al. [44] obtained a similar relation $(\Delta V/V - 3\gamma T) = k\sigma^2$ with the k values of 0.0215 for x=1.2, 0.017 for x=1.6, and 0.0139 for x=1.8, where $\gamma \approx 8.2 \times 10^{-6}$ K^{-1}. Figure 15.14 presents a comparison of the $\Delta V/V$-T and σ^2-T relations, after a thermal expansion correction and an appropriate amplification. A satisfactory agreement between the two sets of data is observed in the whole temperature range from 20 to 300 K, especially near the Curie temperature, where rapid changes in V and σ take place. The decrease of k with x indicates the weakening of spontaneous magnetostriction, that is, the weakening of the first-order nature of the phase transition. It should be noted that although the second-order nature of the transition prevails for $x > 1.8$, the magnetostriction remains significant. Based on the results shown in the inset in Fig. 15.13, magnetostriction could exist up to a x value as high as ~2.4.

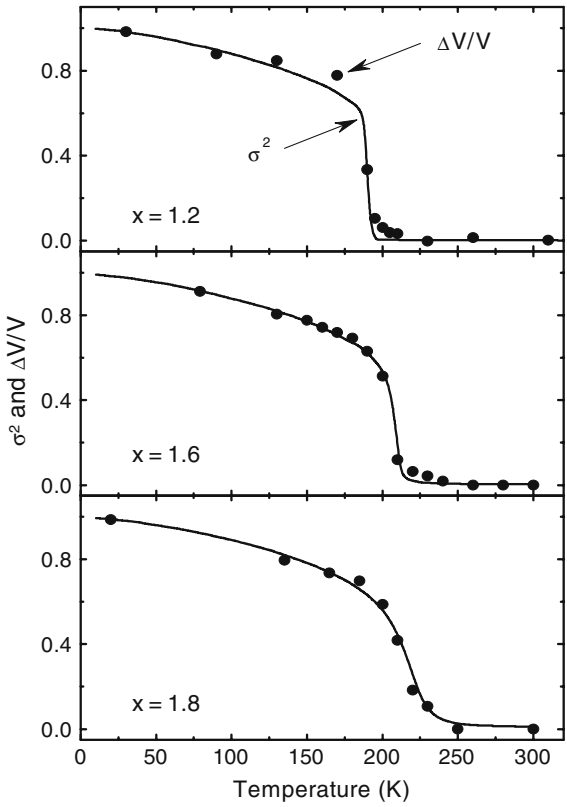

Fig. 15.14
Temperature-dependent normalized thermal magnetization and the lattice constant after thermal expansion correction and proper amplification (Ref. [44])

15.5.1.3 Magnetocaloric effect in $LaFe_{13-x}M_x$ (M = Si, Al, and Co)

Magnetocaloric effect in $LaFe_{13-x}Si_x$

The most attractive property of $LaFe_{13-x}M_x$ is its giant magnetocaloric effect, which did not come into the vision of the people until the work of Hu et al. [16, 17], who observed an entropy change as high as ~20 J/kgK, for a field change of 0−5 T, in $LaFe_{13-x}Si_x$ (x=1.6). This discovery excited a new wave of materials exploration. Figure 15.15 displays the magnetization isotherms of $LaFe_{11.4}Si_{1.6}$ measured in the temperature range from 200 to 255 K. The temperature step is 2 K from 200 to 230 K, 5 K from 165 to 200 K, and from 230 to 255 K. The magnetization is smoothly saturated and its magnitude gradually decreases with increasing temperature below T_C. Above T_C, the $M-H$ cure exhibits a weak "S"-like behavior, which is a signature of IEM transition as explained above.

Magnetic entropy change ΔS can be calculated by Eq. (15.12) based on the data in Fig. 15.15, and the corresponding results are shown in Fig. 15.16 as functions of temperature. The peak values of ΔS for the field changes of 2 T and 5 T are ~10.5

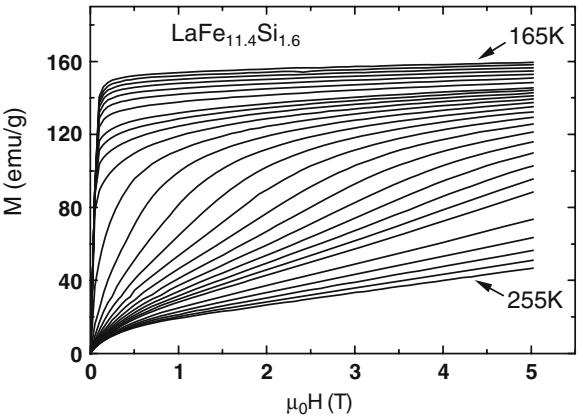

Fig. 15.15 Magnetization isotherms of $LaFe_{11.6}Si_{1.6}$ measured around T_C (Ref. [17])

and ~19.4 J/kg K, respectively, appearing at ~210 K. Such a large $|\Delta S|$ is rare for transition metal alloys in this temperature range.

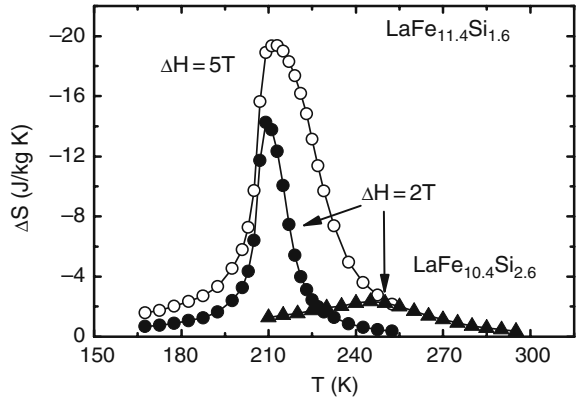

Fig. 15.16 Entropy change of $LaFe_{11.6}Si_{1.6}$ (Ref. [17])

A remarkable phenomenon is the asymmetric broadening of the ΔS peak with applied field. This is a typical feature of first-order phase transition which has a field-dependent critical temperature. It is the increase of T_C with H that yields the expansion of ΔS.

As shown in Section 15.5.1.2, the lattice constant experiences a sudden contraction when the FM to PM transition occurs. The lower the Curie temperature is, the greater the magnetostriction, thus the magnetization change will be. This actually implies that the large entropy change occurs always accompanying a great lattice expansion upon the magnetic transition, as claimed by Hu et al. [17].

Fujieda et al. [45, 46] performed the first measurement of adiabatic temperature change for $LaFe_{13-x}Si_x$ (x=1.3, 1.43, and 1.56) and concluded that the MCE is enhanced as the content of Si decreases. ΔS and ΔT_{ad} for the compound of x=1.56

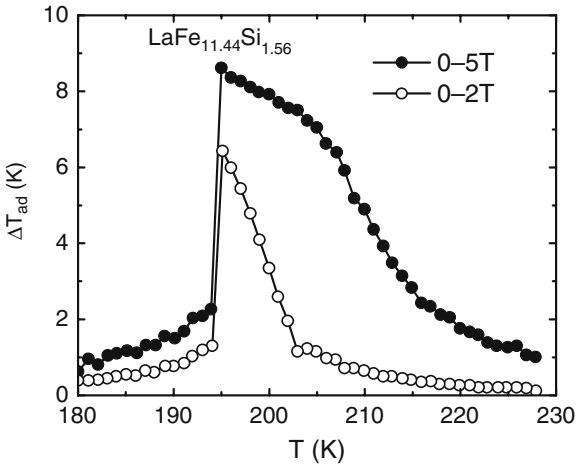

Fig. 15.17 Adiabatic temperature change of $LaFe_{11.44}Si_{1.56}$ for different field changes (Ref. [46])

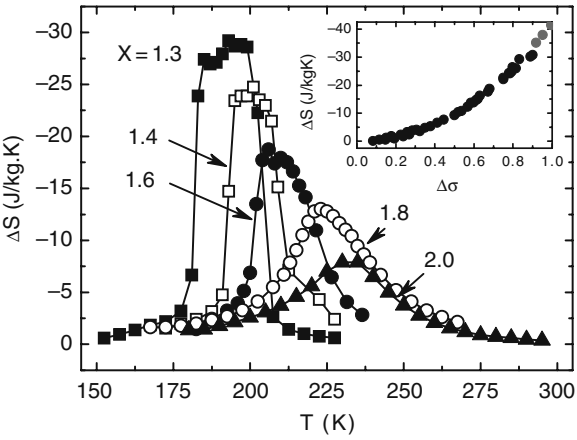

Fig. 15.18 Entropy of $LaFe_{13-x}Si_x$ for a field change of 5 T. Inset plot shows ΔS as a function of σ (Ref. [37])

were found to be ~22.8 J/kgK and ~8.1 K, respectively, by changing the magnetic field from 0 to 2 T, where ΔS has been calculated by Eq. (15.12), and ΔT_{ad} by comparing the $S(T)$ curves (calculated from the heat capacity data) under different magnetic fields as described in Section 15.3.2 (Fig. 15.17).

As mentioned above, MCE enhances as the content of Si decreases. Figure 15.18 displays the typical ΔS–T (ΔH=5 T) relations of $LaFe_{13-x}Si_x$ for x=1.3, 1.4, 1.6, and 2.0 [37]. It is clear that the reduction in x causes a significant decrease in T_C, whereas a rapid increase in ΔS. The maximal ΔS is ~29 J/kgK, appearing at ~190 K when x=1.3. It is unfortunate that the compounds with the Si content lower than 1.2 cannot be obtained. However, by a simple analysis, it can be concluded that the maximal ΔS for $LaFe_{13-x}Si_x$ will be ~40 J/kgK. It is easy to see that there should be a one-to-one correspondence between the field-induced magnetization change ($\Delta\sigma$) and ΔS. By comparing the data of different compounds, a

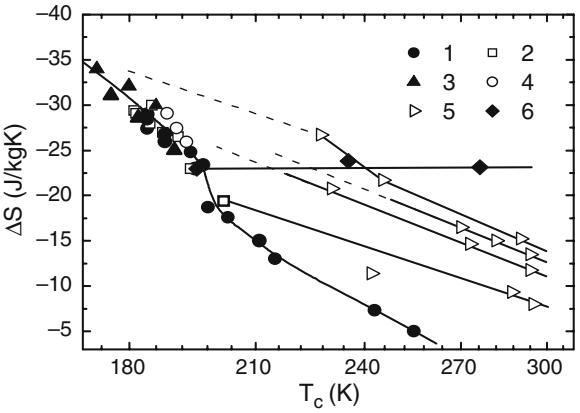

Fig. 15.19 $\Delta S-T_C$ relations for $LaFe_{13}$-based compounds. 1 − $LaFe_{13-x}Si_x$ (Refs. [37, 39]), 2 − $La_{1-z}Pr_zFe_{13-x}Si_x$ (Refs. [58,59,60,61]), 3 − $La_{1-z}Ce_zFe_{13-x}Si_x$ (Refs. [52−56]), 4 − $La_{1-z}Nd_zFe_{13-x}Si_x$(Ref. [57]), 5 − $La_{1-z}Pr_zFe_{13-x-y}Co_ySi_x$ (Ref. [57]), and 6 − $LaFe_{13-x}Si_xH_\delta$ (Ref. [39])

$\Delta S-\Delta\sigma$ relation can be obtained, and the utmost entropy change will be the result corresponding to $\Delta\sigma$=1 (inset in Fig. 15.18). To get a comprehensive picture of ΔS, in Fig. 15.19, we gave a summary for the $T_C\sim\Delta S$ relations of different compounds. It shows the presence of a general correspondence between ΔS and T_C: the former decreases as the latter grows irrespective of whether T_C is modified by the Si or the R content (R = magnetic rare earth, its effects will be discussed below). A remarkable feature is the steep drop of ΔS near ∼194 K. It is a signature of the crossover of the magnetic transition from first order to second order. This result reveals a fact that large entropy changes occur always accompanying the first-order phase transition.

Magnetocaloric Effect in Transition-Metal-Doped $LaFe_{13-x}(Si,Al)_x$

Although the $LaFe_{13-x}Si_x$ compounds exhibit a giant MCE, the ΔS peak usually appears at low temperatures (< 210 K). For the purpose of practical application, it is highly desired that the maximal entropy change can take place near the ambient temperature. According to Fig. 15.19, unfortunately, the MCE weakens rapidly as T_C increases. It is therefore an important issue how to shift T_C to high temperatures without significantly affecting ΔS. Hu et al. [47] found that the best effect can be obtained by replacing Fe with appropriate amount of Co. Figures 15.20 and 15.21 display the magnetization isotherms and the corresponding entropy change of $La(Fe_{1-x}Co_x)_{11.9}Si_{1.1}$ (x=0.04, 0.06 and 0.08), respectively. The Curie temperature increases from 240 to 293 K as x increases from 0.02 to 0.08, while only a slow decrease of ΔS from ∼23 to ∼15.6 J/kgK (ΔH=5 T). It is noteworthy that the sample with x=0.6 shows nearly the same ΔS (∼ 20 J/kgK at ∼ 274 K) as that of $Gd_5Si_2Ge_2$ and $MnFeP_{0.45}As_{0.55}$ whereas there is no obvious magnetic hysteresis, which is highly desired by practical application. Similar results were obtained by other groups [48]. Substituting Fe with Co in $LaFe_{11.2}Si_{1.8}$ and $La_{0.6}Pr_{0.4}Fe_{11.2}Si_{1.8}$, the former exhibits a second-order transition, results in similar effects as those described above. It is interesting to note that the $\Delta S-T_C$ curves obtained by varying

Co content while fixing the Si content are nearly parallel with each other (marked by the open triangles in Fig. 15.19).

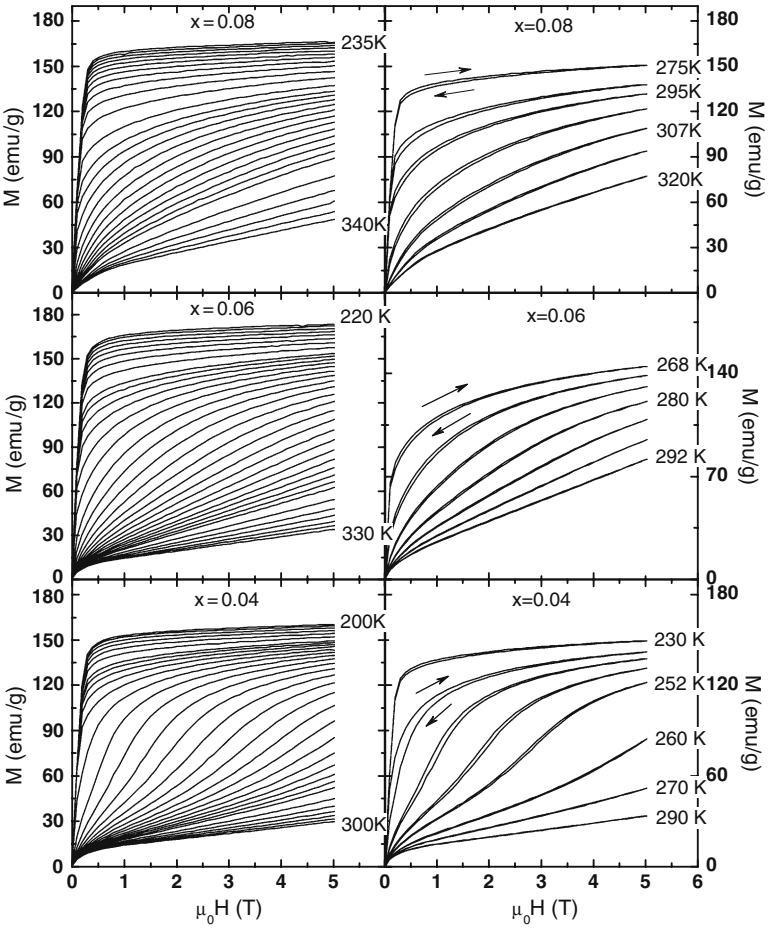

Fig. 15.20 Magnetization isotherms of $La(Fe_{1-x}Co_x)_{11.9}Si_{1.1}$ (Ref. [47])

Although both the Si-doping and the Co-doping drive T_C to high temperatures, the reduction of ΔS is much slower in the latter case. According to Fig. 15.19, ΔS is ~22 J/kgK for $La_{0.8}Ce_{0.2}Fe_{11.7-y}Co_ySi_{1.3}$ and ~7 J/kgK for $LaFe_{13-x}Si_x$ (x=2.4), while T_C takes nearly the same value of ~242 K. Therefore, reducing the Si content in $LaFe_{13-x}Si_x$ as low as possibly and partial replacing Fe by Co is a promising way to get room temperature giant MCE.

Hu et al. [42] found that partial replacement of Fe with Co droved the samples from the AFM to the FM state and, similar to $LaFe_{13-x}Si_x$, T_C shifts to high temperatures when the Co content increases. A distinctive feature is that the entropy

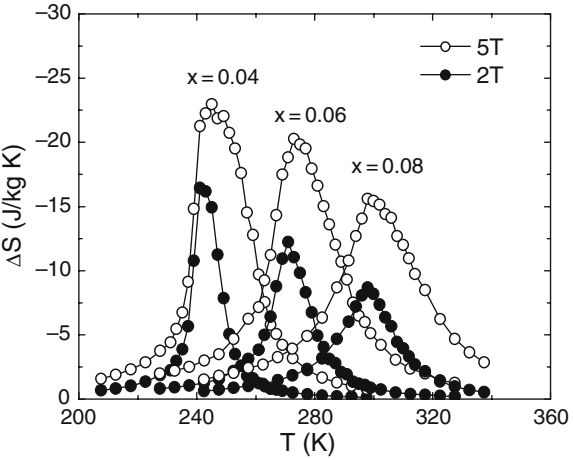

Fig. 15.21 Entropy changes of $La(Fe_{1-x}Co_x)_{11.9}Si_{1.1}$ (Ref. [47])

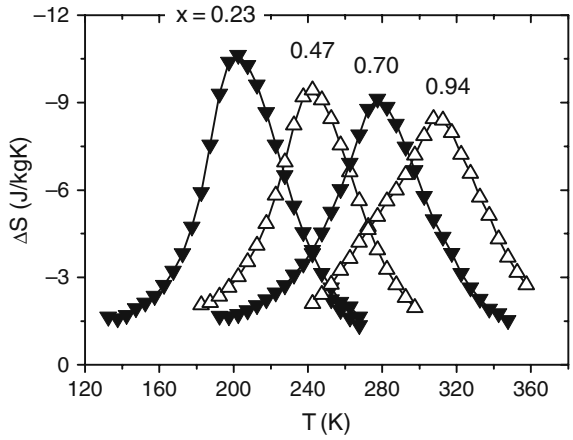

Fig. 15.22 Entropy change of $LaFe_{13-x}Co_xAl_{1.3}$ (Ref. [37])

change keeps nearly constant as Curie temperature grows, though the value of ΔS is not very large. Figure 15.22 shows the entropy change of $LaFe_{11.7-y}Co_yAl_{1.3}$ with different Co contents.

In an attempt to find out a way to depress T_C while effectively retaining the large ΔS, Wang et al. [49] studied the effect of substituting Fe by Mn, which may have a AFM coupling with adjacent Fe. The Mn content in $LaFe_{11.7-y}Mn_ySi_{1.3}$ is y=0, 0.117, 0.234, and 0.351. The cubic $NaZn_{13}$-type structure keeps unchanged except for the appearance of minor α-Fe phase (< 5 wt%) for $x \geq 0.234$. A decrease in saturation magnetization much larger than that expected by a simple dilution effect is observed, which is consistent with the anticipated antiparallel arrangements of Fe and Mn (Fig. 15.23). The Curie temperature is found to decrease linearly at a rate of ∼174 K for 1% Mn. A large ΔS is gained in a wide temperature range,

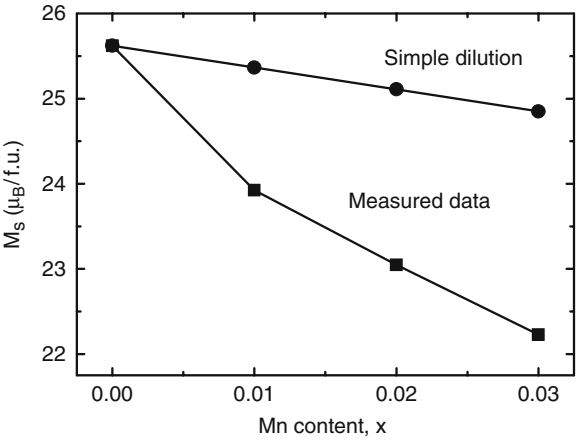

Fig. 15.23 Saturation magnetization of $LaFe_{13-x}Mn_xSi_{1.3}$ (Ref. [75])

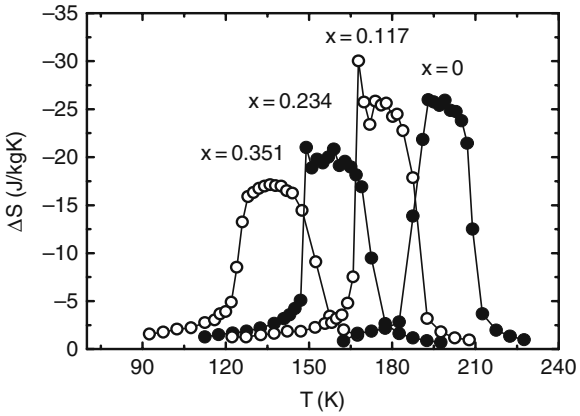

Fig. 15.24 Entropy change of $LaFe_{13-x}Mn_xSi_{1.3}$ (ΔH=5 T) (Ref. [75])

though a tendency toward degeneration appears as y increases (Fig. 15.24). It is ~17 J/kgK for T_C=130 K and ~25 J/kgK for T_C=188 K, for a field change of 0−5 T. Increase of the temperature span of ΔS is obvious. It is ~21.5 K for y=0 and ~31.5 K for y=0.351 (ΔH=5 T). Fujieda et al. [50] observed similar phenomena in $La_{1-z}Ce_zFe_{13-x-y}Mn_ySi_x$. When the content of Mn is high enough (y > 0.9), long-range FM order will be destroyed, and typical spin glass behavior appears [49].

Magnetocaloric Effect in Magnetic Rare-Earth-Doped $LaFe_{13-x}Si_x$

Effects of magnetic rare-earth (R) doping were first studied by Anh et al. in 2003 [51]. The authors declared an increase of T_C and a decrease of MCE in $La_{1-z}Nd_zFe_{11.44}Si_{1.56}$ (z=0−0.4) with the incorporation of Nd. However, these results are inconsistent with those subsequently obtained by other groups. Fujieda

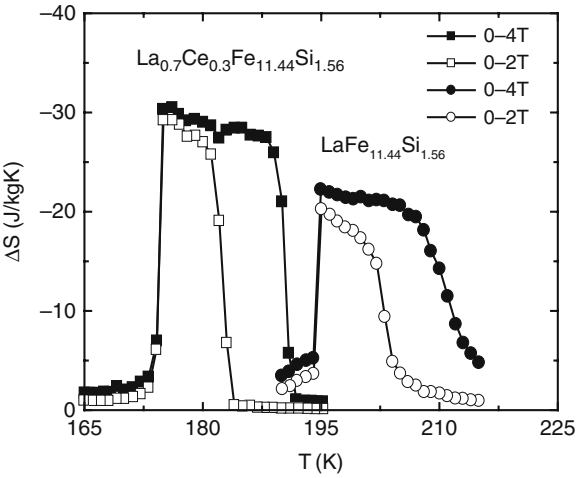

Fig. 15.25 Temperature dependence of the entropy changes of $LaFe_{11.44}Si_{1.56}$ and $La_{0.7}Ce_{0.3}Fe_{11.44}Si_{1.56}$ (Ref. [54])

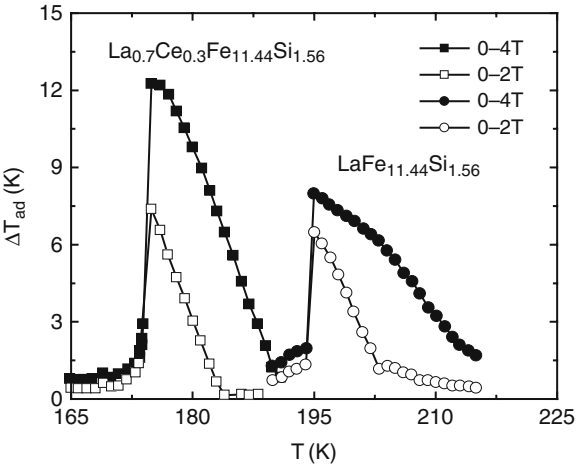

Fig. 15.26 Adiabatic temperature change of $LaFe_{11.44}Si_{1.56}$ and $La_{0.7}Ce_{0.3}Fe_{11.44}Si_{1.56}$ (Ref. [54])

et al. [52−56] performed a systematic study on the effect of Ce-doping for the compounds $LaFe_{13-x}Si_x$ with x=1.3, 1.56, and 1.82. There is a limitation to the content of R in the compound, beyond which impurity phases will appear. The maximal Ce content studied is 0.3. There are two remarkable observations. The first one is the low temperature shift of T_C and the second one is the enhancement of MCE with the incorporation of Ce. The entropy and adiabatic temperature changes of $La_{0.7}Ce_{0.3}Fe_{11.44}Si_{1.56}$ are, respectively, shown in Figs. 15.25 and 15.26. Results without Ce are also presented for comparison. It indicates that the presence of 30% Ce reduces T_C by ∼24 K whereas increases ΔS by ∼8 J/kgK (ΔH=4 T). The maximal entropy change is ∼34 J/kgK, appearing in $La_{0.9}Ce_{0.2}Fe_{11.7}Si_{1.3}$. Effects of other magnetic rare earths were also studied, such as Nd, by Shen et al. [58], and Pr, by

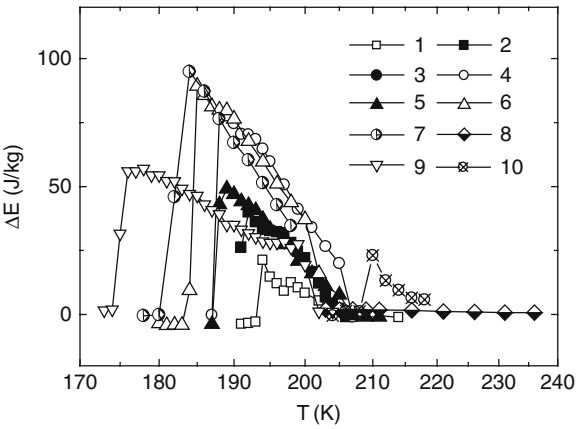

Fig. 15.27 Magnetic hysteresis loss in $LaFe_{13}$-based compounds (unpublished data of the authors). 1 − $LaFe_{11.5}Si_{1.5}$, 2 − $La_{0.9}Nd_{0.1}Fe_{11.5}Si_{1.5}$, 3 − $La_{0.8}Nd_{0.2}Fe_{11.5}Si_{1.5}$, 4 − $La_{0.7}Nd_{0.3}Fe_{11.5}Si_{1.5}$, 5 − $La_{0.8}Pr_{0.2}Fe_{11.5}Si_{1.5}$, 6 − $La_{0.7}Pr_{0.3}Fe_{11.5}Si_{1.5}$, 7 − $La_{0.5}Pr_{0.5}Fe_{11.5}Si_{1.5}$, 8 − $La_{0.7}Pr_{0.3}Fe_{11.5}Si_{1.5}$, 9 − $LaFe_{11.83}Si_{1.17}$, and 10 − $La_{0.5}Pr_{0.5}Fe_{11.5}Si_{1.5}C_{0.3}$

Shen et al. [58] and Fujieda et al. [59, 60]. Fujieda et al. [59] successfully extended the content of Pr up to 0.7 when Si content is 1.82. Analyses of these results lead to the following conclusions: (i) the incorporation of magnetic rare earth causes a low temperature shift of T_C, thus a strengthening the first-order nature of the phase transition. Sometimes a second-order phase transition becomes first order after the introduction of R. (ii) The MCE enhances with the increase of the R content.

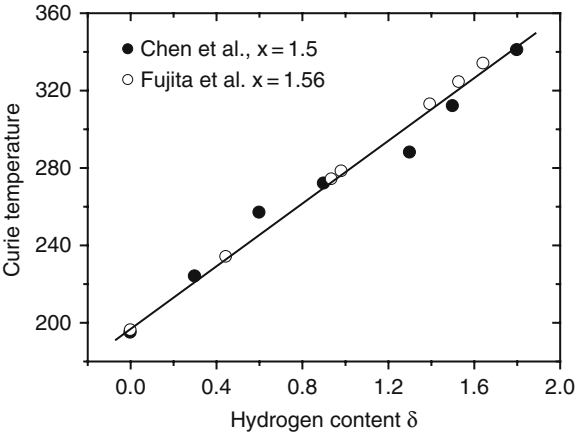

Fig. 15.28 Curie temperature as a function of hydrogen concentration. Data were obtained from Refs. [66] and [39] for x=1.5 and 1.56, respectively

It is obvious that the enhancement of MCE occurs accompanying the decrease of T_C, which can be realized by tuning the content of R or Si. It would be instructive to analyze the $\Delta S - T_C$ relations resulted by changing Si content without introducing R or changing R content while keeping the Si concentration constant, which will allow a comparison of the ΔS values at the same temperature. A remarkable observation is the equivalence of increasing z to reducing x, as demonstrated by the coincidence of the two sets of data in Fig. 15.19.

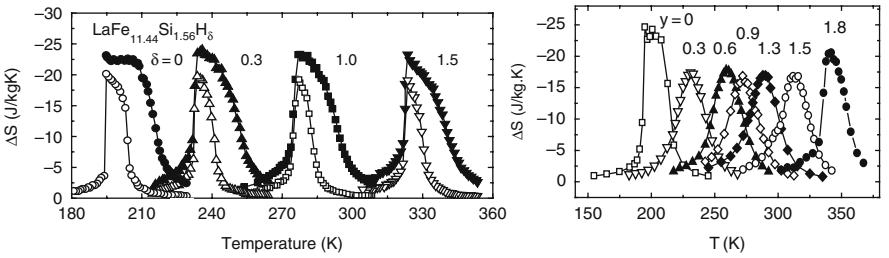

Fig. 15.29 Entropy change of the hydrides $LaFe_{11.44}Si_{1.56}H_\delta$(*left*, Ref. [39]) and $LaFe_{11.5}Si_{1.5}H_\delta$ (*right*, Ref. [66]) (ΔH=5 T)

Although R and Si have similar effects on ΔS, their influence on magnetic hysteresis is different. Defining the energy loss (ΔE) due to magnetic hysteresis as the area encircled by the two magnetization isotherms, we obtained the $\Delta E-T$ relation shown in Fig. 15.27, based on the data of different compounds $La_{1-z}R_zFe_{13-x}Si_x$. It is clear that ΔE is negligible for $T > 220$ K and increases rapidly as T decreases. Comparing the hysteresis loss at the same temperature, it can be seen that ΔE increases when R is introduced. This conclusion is different from that of Fujieda et al. [53], who claimed a depression of ΔE in $La_{0.7}Ce_{0.3}Fe_{11.18}Si_{1.82}$ compared with $LaFe_{11.44}Si_{1.56}$. The disappearance of ΔE demonstrates again the prevalence of the second-order transition above 210 K.

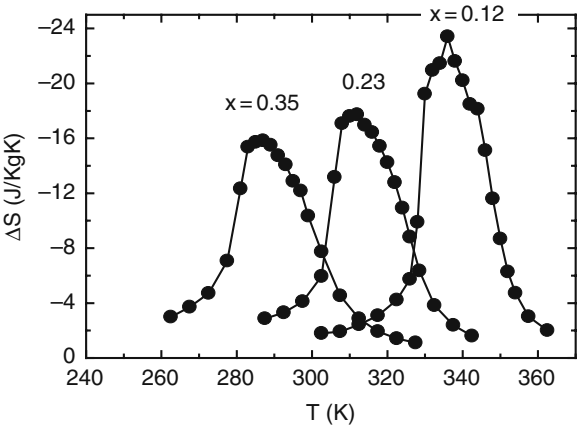

Fig. 15.30 Entropy change of the $LaFe_{11.7-x}Mn_xSi_{1.3}H_\delta$ hydrides (ΔH=5 T)

Interstitial Effect in $La(Fe_{1-x}Si_x)_{13}$

For the purpose of practical application, as mentioned in the previous sections, it is required that the giant MCE can occur near the ambient temperature. However, as shown in Fig. 15.19, ΔS decreases rapidly as T_C increases for the $LaFe_{13-x}Si_x$ compounds. It is therefore highly desired to find out an effective approach to push

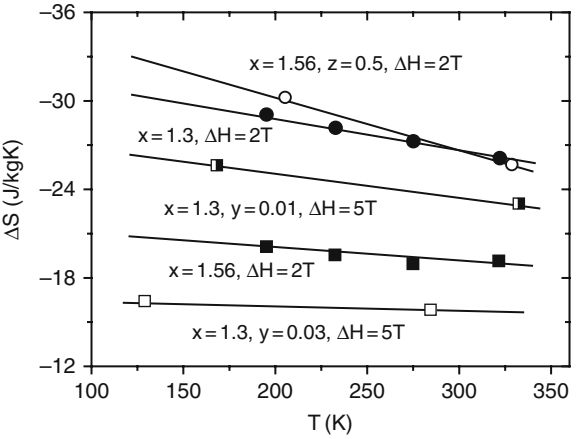

Fig. 15.31 Entropy changes of $La_{1-z}Pr_zFe_{11.44}Si_{1.56}H_\delta$ for z=0 (Ref. [39]) and 0.5 (Ref. [76]) and $LaFe_{11.7-y}Mn_ySi_{1.3}H_\delta$ for y=0 (Ref. [75]) and y=0.117 and 0.234 (Ref. [77]).

ΔS to high temperatures without reducing its height. Fujieda et al. [62,63,64] and Chen et al. [65, 66] independently found that the incorporation of interstitial hydrogen shifted T_C to high temperatures, while the MCE essentially remains. The effects are completely different from those of replacing Fe with Co, Ni, Si, or Al and were inattentive before, though magnetic properties of the relevant nitrides [67,68,69,70] and hydrides [71, 72] have been studied since 1993.

By changing either the pressure of hydrogen atmosphere or annealing temperature, the concentration of interstitial hydrogen in $LaFe_{13-x}Si_xH_\delta$ was controlled by Fujieda et al. [39]. The hydrogen concentration was determined by both gas chromatograph and gas fusion analyses. In contrast, Chen et al. [65, 66] tuned the content of hydrogen by carefully regulating the desorption of absorbed hydrogen. The Curie temperature was found to increase linearly with the content of hydrogen, while the magnetic transition remains first order. This is completely different from the effect of Si- and/or Co doping, which causes an evolution of magnetic transition from first order to second order. In this way, the giant MCE that usually appears at low temperatures can be pushed toward high temperatures. Figure 15.28 shows the variation of T_C with δ. The effect of interstitial atom on T_C is similar for the La(Fe, $Si)_{13}H_\delta$ hydrides and other R−Fe-based interstitial compounds, for which lattice expansion caused by interstitial atoms depresses the overlap between Fe-3d electrons, thus leads to a reduction of T_C [65–70].

The typical entropy changes of $LaFe_{13-x}Si_x$ for x=1.5 [66] and 1.56 [39] are shown in Fig. 15.29. The peak height of ΔS keeps at ∼23 J/kgK (ΔH = 5 T) for x=1.56 as T_C increases from ∼195 to ∼330 K. Due to the broadening of magnetic transition caused by hydrogen desorption, the ΔS value in $LaFe_{11.5}Si_{1.5}$ is somewhat lower in the intermediated hydrogen concentration range.

Fukamichi et al. [73] further studied the effect of interstitial hydrogen for $LaFe_{13-x}Si_x$ with x=1.3, which exhibits a much larger ΔS. It was found that ΔS, for a field change of 0−2 T, varied from ∼29 J/kgK for T≈195 K to ∼26 J/kgK

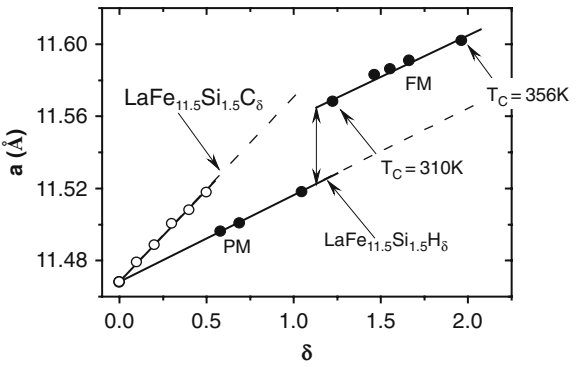

Fig. 15.32 Lattice constant as a function of the content of interstitial atoms for $LaFe_{11.5}Si_{1.5}(H/C)_{\delta}$ (Ref. [77])

for $T \approx 320$ K, again a slow decay of ΔS with T_C. Influence of interstitial atoms on MCE was also investigated for $La_{1-x}Pr_xFe_{11.44}Si_{1.56}$ [74]. The decrease of ΔS with the increase of T_C is more rapid compared with other compounds without R, as shown in Fig. 15.31, which could be a consequence of the broadening of magnetic transition due to the bad crystal quality of the samples. Wang et al. [75] studied the MCE of the $LaFe_{11.7-y}Mn_ySi_{1.3}H_{\delta}$ hydride (Fig. 15.30), which exhibits a much lower T_C, and obtained the same conclusion that the incorporation of interstitial hydrogen drives ΔS to higher temperatures at the least expense of ΔS value (Fig. 15.31). According to Fig. 15.31, the Curie temperature of $LaFe_{13-x}Si_xH_{\delta}$ can be tuned between ~130 and ~340 K by the content of hydrogen while large ΔS retains.

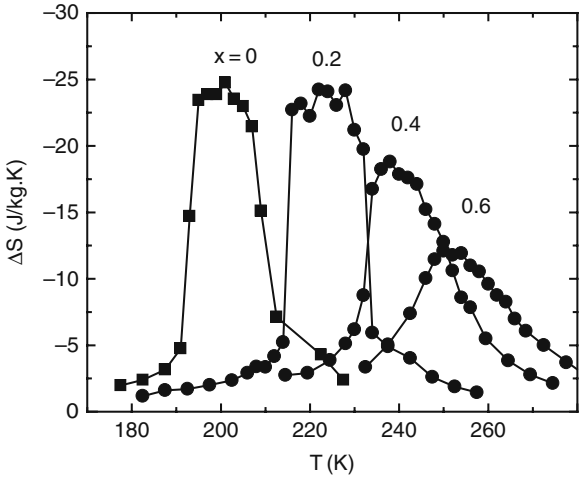

Fig. 15.33 Entropy change of $LaFe_{11.5}Si_{1.5}C_{\delta}$ (ΔH=5 T) (Ref. [78])

It is unfortunate that the hydrides are usually chemically unstable above 150°C, which could be a fatal problem for practical applications. It is therefore necessary to develop chemically stable interstitials with high T_Cs and great ΔS values. Chen

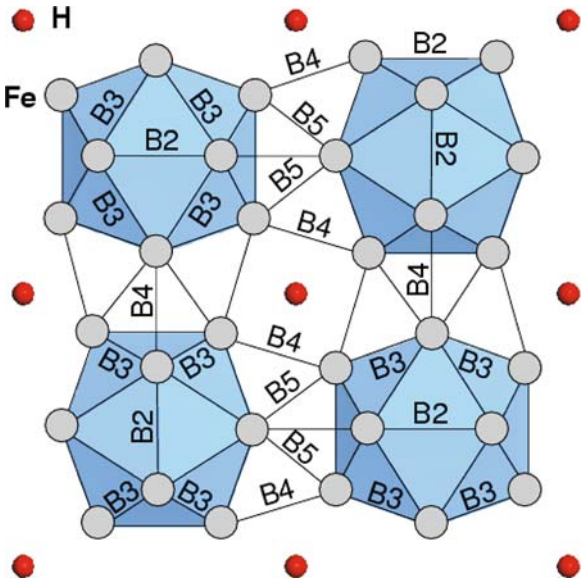

Fig. 15.34 A schematic for the atomic structure of $LaFe_{13}H_3$ (La is omitted for clarity) (Ref. [77])

et al. [76] studied the effects of interstitial carbon for the $LaFe_{13-x}Si_xC_\delta$ carbides, which are stable up to the melting point. The $LaFe_{11.4}Si_{1.4}C_\delta$ (δ=0, 0.2, 0.4, and 0.6) carbides were prepared by the solid–solid phase reaction technique, that is, arc melting Fe−C intermediate alloy together with La, Fe and Si. X-ray diffraction analyses indicate the volume expansions of ∼0.29, ∼0.75, and ∼0.93% corresponding to δ=0.2, 0.4, and 0.6, respectively, though the cubic $NaZn_{13}$-type structure remains unchanged. Compared with hydrides, the lattice expansion of carbides is much stronger [77], as shown in Fig. 15.32. Minor α-Fe phase appears (6%) when the carbon concentration is δ=0.6. The Curie temperatures of $LaFe_{11.6}Si_{1.4}C_x$ are 195, 218, 238, and 250 K for δ=0, 0.2, 0.4, and 0.6, respectively, increasing with carbon content.

Figure 15.33 shows the entropy change of $LaFe_{11.6}Si_{1.4}C_\delta$ [76]. The maximal ΔS is ∼24.2 J/kgK for δ=0.2, ∼18.8 J/kgK for δ=0.4, and ∼12.1 J/kgK for x=0.6. The entropy change remains constant when x is below 0.2, while decreases rapidly for $x > 0.4$. The latter could be a consequence of the appearance of impurity phase, which affects crystal quality of the sample, thus broadens the phase transition. A little different carbides $LaFe_{11.5}Si_{1.5}C_\delta$ were also studied and similar effects were observed.

Structure changes due to the introduction of hydrogen were studied by Jia et al. [77] for the $LaFe_{11.5}Si_{1.5}H_\delta$ hydrides (δ=0, 1.2, and 2), based on the Rietveld analyses of powder X-ray diffraction spectra. It was found that the incorporation of interstitial atoms causes a lattice expansion of the compounds while leaves the structural symmetry unchanged. Accompanying the lattice expansion, as shown in Figs. 15.34 and 15.35, Fe−Fe bond exhibits a concomitant variation. Four of the

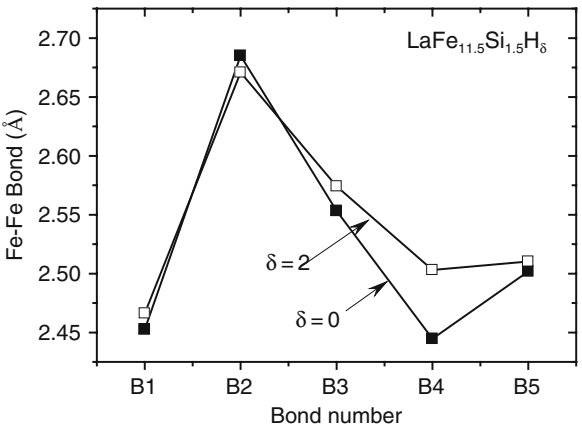

Fig. 15.35 Change of Fe−Fe bond length upon hydrogenating for the compound $LaFe_{11.5}Si_{1.5}H_{\delta}$ (Ref. [77])

five Fe−Fe bonds show a tendency to expansion. The largest elongation occurs for the shortest inter-cluster bond (B_4), and the relative change is as large as ∼2.37% as δ increases from 0 to 2. In contrast, the longest Fe−Fe bond (B_2) shrinks considerably (−0.53%). Effect of Ce doping was also studied by the same authors for comparison. It is fascinating that the increase in Ce content produces essentially the same effect on Fe−Fe bonds as the decrease of hydrogen content, though interstitial atoms occupy different crystallographic sites from rare earths. A linear increase of Curie temperature with lattice constant, at a rate of ∼1,779 K/Å for $LaFe_{11.5}Si_{1.5}H_{\delta}/La_{1-x}Ce_xFe_{11.5}Si_{1.5}$ and ∼1,089 K/Å for $LaFe_{11.5}Si_{1.5}C_{\delta}$, is observed. This is a signature of the strengthening of magnetic coupling as lattice expands. It is found that the change of the shortest Fe−Fe bond dominates the magnetic coupling in the $LaFe_{1\,s-x}Si_x$-based intermetallics. A relation between exchange integral and Fe−Fe distance has been proposed to explain the volume effects observed.

In Table 15.1, we give a summary of the magnetic/crystallographic transition temperature T_C, isothermal entropy change ΔS, adiabatic temperature change $\Delta T_{ad}$for $LaFe_{13-x}Si_x$, and related compounds.

Thermal and Magnetic Hystereses of $La(Fe_{1-x}Si_x)_{13}$

A typical feature of the first-order transition is the appearance of thermal and magnetic hystereses. This will affect the efficiency of magnetic refrigeration. As mentioned in previous sections, although MCE enhances in the materials that show first-order transitions, thermal and magnetic hystereses intensify simultaneously. This phenomenon is especially obvious in R-doped $LaFe_{13-x}Si_x$, $Gd_5(Si_{1-x}Ge_x)_4$ and MnAs-based compounds. It is therefore necessary to find a method to depress magnetic hysteresis without spoiling the giant MCE, which is actually equivalent to depressing the driving force of the phase transition. Recently Shen et al. [78] found that the hysteresis can be significantly depressed by introducing

Table 15.1 Magnetic/crystallographic transition temperature T_C, isothermal entropy change ΔS, adiabatic temperature change $\Delta T_{ad}$for $LaFe_{13-x}Si_x$, and related compounds for the field changes from 0 to 2 T and from 0 to 5 T

Material	T_C (K)	ΔS(J/kgK) (0−2 T)	ΔS (J/kgK) (0−5 T)	ΔT_{ad} (K) (0−2 T)	ΔT_{ad} (K) (0−5 T)	References
$LaFe_{13-x}Si_x$						
x = 1.3	184	−28	−30		12.1	[39]
x = 1.43	188	−24	−26		10.7	[39]
x = 1.56	195	−20	−23	6.5	8.6	[39, 56]
x = 1.6	208	−14				[37]
x = 1.8	220	−7.48	−13			[37]
x = 2.0	234	−4	−7.2			[37]
x = 2.4	250	−3	−4.8			[37, 79]
$La_{1-x}Ce_xFe_{11.44}Si_{1.56}$						
x = 0.1		−22.9				[53, 54]
x = 0.2		−26.4				[53, 54]
x = 0.3		−28.9		7.3		[53, 54]
$La_{1-z}Pr_zFe_{11.5}Si_{1.5}$						
Z = 0.1	191.0		−16.5			[57]
Z = 0.2	187.5		−27.0			[57]
Z = 0.3	184.5		−28.0			[57]
Z = 0.4	181.5		−29.1			[57]
Z = 0.5	181.0		−29.4			[57]
$La_{1-x}Pr_xFe_{11.44}Si_{1.56}$						
Z = 0	195.9		−23.0		8.6	[74]
Z = 0.1	193.8		−25.7		10.5	[74]
Z = 0.2	192.2		−25.4		10.4	[74]
Z = 0.3	191.1		−26.0		11	[74]
Z = 0.4	188.0		−27.5		11.3	[74]
Z = 0.5	186.1		−29.9		11.9	[74]
$LaFe_{11.7}Si_{1.3}H_\delta$						
δ = 1.1	287	−28	−31	7.1	15.4	[39]

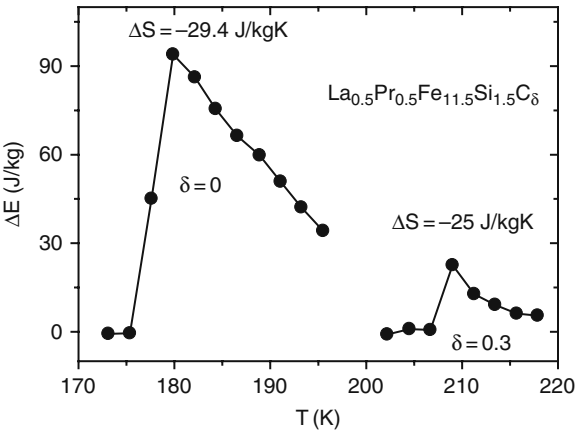

Fig. 15.36 Temperature-dependent hysteresis loss of $La_{0.5}Pr_{0.5}Fe_{11.5}Si_{1.5}C_\delta$ (δ=0 and 0.3) (Ref. [78])

interstitial atoms into the compound. Figure 15.36 displays the hysteresis loss of $La_{0.5}Pr_{0.5}Fe_{11.5}Si_{1.5}C_{\delta}$. ΔE decreases from ~91 to ~22 J/kgK when δ increases from 0 to 0.3. The high-temperature shift of the phase transition, where the maximal ΔS occurs, could be the main reason for the reduction of ΔE: Strong thermal fluctuation at high temperatures reduces the driving force required. This result indicates that introducing interstitial atoms could be also be a promising method to get giant MCE while without significant ΔE.

15.5.2 $Gd_5(Ge,Si)_4$ and Related Compounds

The large entropy change observed in $Gd_5Si_2Ge_2$ [14, 15] triggered the exploration of the MCE effect in $Gd_5(Ge,Si)_4$ and related compounds [80,82,83,84,85]. In the following, we will give a brief introduction to this kind of materials. A detailed review can be found elsewhere [86]. In fact, the crystal structures of Gd_5Si_4, Gd_5Ge_4 and $Gd_5(Ge,Si)_4$ were studied 40 years ago [87], and three categories of structures were identified, which are, respectively, the Gd_5Si_4- and Gd_5Ge_4-based structures, and an unknown phase when the Ge or Si content is in the intermediate range. It was originally believed that the Gd_5Si_4 and Gd_5Ge_4-based solutions have the Sm_5Ge_4-type structure. A completed phase diagram of the $Gd_5(Si_xGe_{1-x})_4$system was recently established by Pecharsky and Gschneidner [80]. Three extended solid solution regions and two two-phase coexisted regions were confirmed, see Fig. 15.37. The first one is Si-rich region when $0.575 \leq x \leq 1$. The compounds in this region crystallize in the Gd_5Si_4structure and they undergo a second-order magnetic transition on warming, without structural changes. All of the compounds exhibit a moderate MCE. The second region is for $0.4 < x \leq 0.503$, where the $Gd_5Si_2Ge_2$-type solid solutions with monoclinic structure appear. The alloys in this region experience a first-order magnetic transition that is coupled with a $Gd_5Si_4$to $Gd_5Si_2Ge_2$structure change and display a giant MCE. The last region is for $0 < x \leq 0.3$, where the Sm_5Ge_4-type structure is supported. Two regions with coexisted phases were also identified. The first one is the coexistence of the Sm_5Ge_4-type and the $Gd_5Si_2Ge_2$-type phases when $0.3 < x \leq 0.4$, and second one is the coexistent $Gd_5Si_2Ge_2$-type and Gd_5Si_4-type structure when $0.503 < x < 0.575$. Both the monoclinic $Gd_5Si_2Ge_2$-type and the orthorhombic Sm_5Ge_4-type alloys exhibit giant MCE around respective transition temperatures because of the first-order phase transformations.

The major difference between the three crystallographic modifications in the $Gd_5(Si_xGe_{1-x})_4$ system is due to different bonding arrangements between the well-defined sub-nanometer thick slabs [80]. The orthorhombic Sm_5Ge_4type, where none of the slabs are interconnected via covalent-like Ge−Ge bonds, belongs to space group *Pnma*. The $Gd_5Si_2Ge_2$type is the monoclinic phase, which belongs to space group *P*112/*a*, and the covalent-like (Si,Ge)−(Si,Ge) bonds connect the slabs into pairs, but no (Si,Ge)−(Si,Ge) bonds are found between the pairs of the slabs. The Gd_5Si_4type is also an orthorhombic structure and it has the same space group as

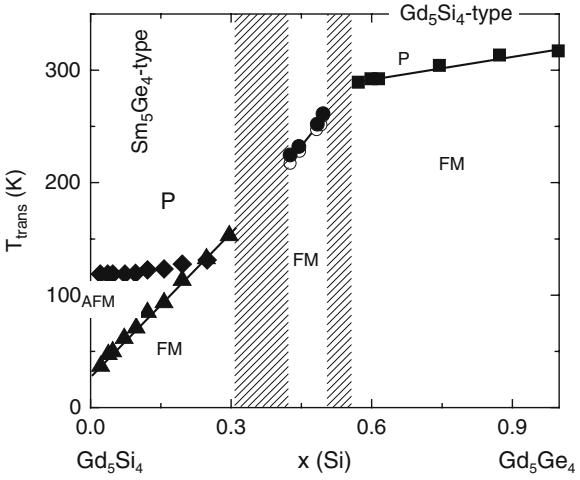

Fig. 15.37 Magnetic phase diagram of the $Gd_5Si_4-Gd_5Ge_4$ pseudobinary system. The *thin solid lines* indicate magnetic phase boundaries, and the *vertical dotted lines* delineate the regions where the alloys are single-phase materials (the compositions within *shaded areas* are two-phase alloys). This figure is reprinted from Ref. [80]

the Sm_5Ge_4-type structure, but all the slabs are interconnected via covalent-like Si−Si bonds. During the Gd_5Si_4-type to Sm_5Ge_4-type phase change, the a lattice parameter expansion exceeds that of the other two lattice parameters by nearly a factor of 5. On the atomic resolution scale, the distances between the Si(Ge) atoms increase from 2.5 to 2.6 Å (Gd_5Si_4) to 3.4−3.5 Å (Gd_5Ge_4), indicating much stronger interactions between the slabs in the former when compared with the latter.

The structural change at the phase transition in the $Gd_5(Si_xGe_{1-x})_4$ system also brings about a strong magneto-elastic effect, and an anomalous electrical resistivity, indicating a strong coupling between electronic structure and lattice.

Because of the coupled magnetic and structural transitions, $Gd_5(Si_xGe_{1-x})_4$ exhibits great magnetic entropy change ΔS covering the temperatures from ∼50 to ∼300 K [15]. The ΔS value first reported in a polycrystalline sample $Gd_5Si_2Ge_2$[14] in 1997 reached 18.8 J/kgK for a field change of 5 T, and the corresponding adiabatic temperature change is 15 K. It is nearly doubled the MCE of the known materials at that time. By improving the crystal quality of $Gd_5Si_2Ge_2$, the ΔS value was further enhanced by 80% and ΔT_{ad} by 55% [87]. A minor addition of other elements such as Fe, Co, Ni, Cu, Ga, Al, and C can shift the temperature of the phase transition but did not enhance the MCE effect [88]. By altering the Si to Ge ratio in $Gd_5(Si_xGe_{1-x})_4$, the transition temperature shifts from ∼50 to ∼300 K, and a great MCE was resulted (Fig. 15.38).

Although the $Gd_5(Si_xGe_{1-x})_4$ system shows a great MCE, it exhibits considerable magnetic and thermal hystereses, which will impede its practical application as refrigerants. It is therefore necessary to reduce hysteresis loss while retaining the MCE. Unfortunately, a satisfy solution cannot be found in literature. Although changing the Si to Ge ratio can push T_C to high temperatures, no significant improvement in hysteresis loss was observed. It was recently reported that the addition

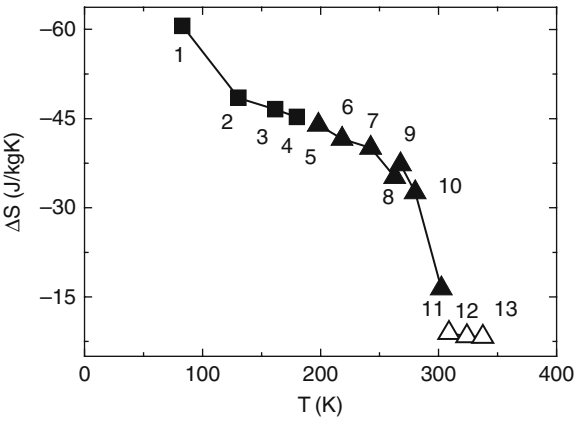

Fig. 15.38 Magnetic entropy change of the $Gd_5(Si_xGe_{1-x})_4$ for a field change of 5 T. *Solid squares* are for the compounds which exhibit a coupled magnetic and structural transition; *solid triangles* represent those for the first-order magnetic transition coupled with Gd_5Si_4-type to $Gd_5Si_2Ge_2$-type structural transformation, while the open triangles are for the second-order ferromagnetic–paramagnetic transition with Gd_5Si_4-type structure unchanged. The data of this figure were obtained from Ref. [86]. 1 − $Gd_5Si_{0.5}Ge_{3.5}$, 2 − Gd_5SiGe_3, 3 − $Gd_5Si_{1.2}Ge_{2.8}$, 4 − $Gd_5Si_{1.3}Ge_{2.7}$, 5 − $Gd_5Si_{1.5}Ge_{2.5}$, 6 − $Gd_5Si_{1.6}Ge_{2.4}$, 7 − $Gd_5Si_{1.8}Ge_{2.2}$, 8 − $Gd_5Si_{1.95}Ge_{2.05}$, 9 − $Gd_5Si_{1.98}Ge_{2.02}$, 10 − $Gd_5Si_{2.02}Ge_{1.98}$, 11 − $Gd_5Si_{2.1}Ge_{1.9}$, 12 − $Gd_5Si_{2.3}Ge_{1.7}$, 13 − Gd_5Si_3Ge, and 14 − Gd_5Si_4

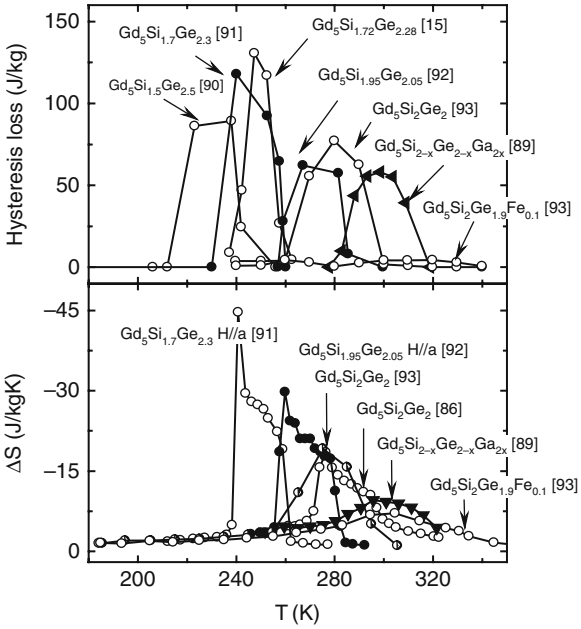

Fig. 15.39 Magnetic hysteresis loss (*top panel*) and magnetic entropy change (*bottom panel*) as functions of temperature for the $Gd_5(Si_{1-x}Ge_x)_4$ compounds (unpublished data of the authors)

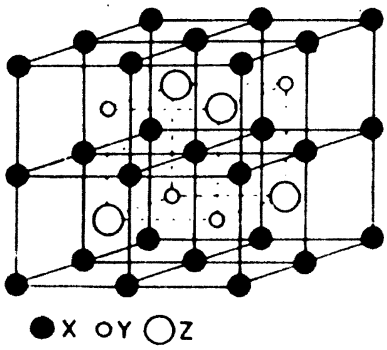

Fig. 15.40 A schematic structure of Heusler alloy X_2YZ

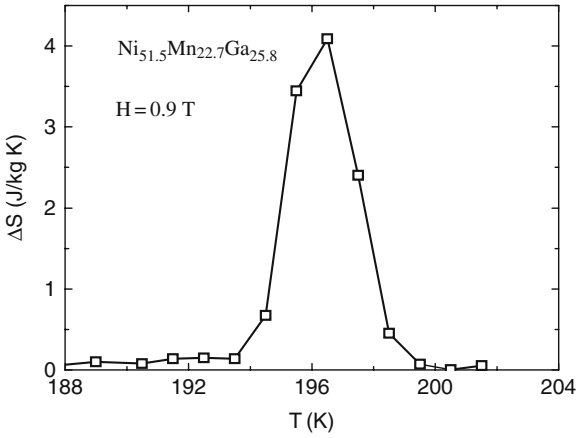

Fig. 15.41 Magnetic entropy change of a polycrystalline alloy $Ni_{51.5}Mn_{22.7}Ga_{25.8}$ under a field change from 0 to 0.9 T (Ref. [96])

of Fe can remarkably reduce the hysteresis loss, however, ΔS was simultaneously depressed by 63% [93]. Figures 15.39(a) and (b) show the magnetic hysteresis loss and the entropy change as functions of temperature for the $Gd_5(Si_xGe_{1-x})_4$ compounds.

For practical applications, the production cost of the refrigerant is also an important factor to be considered. It has been reported that the MCE of $Gd_5(Si_xGe_{1-x})_4$ depends strongly on the purity of starting materials [88]. Impurity atoms such as carbon and oxygen in the starting materials can hamper the formation of the monoclinic structure, and the $Gd_5(Si_xGe_{1-x})_4$alloys thus obtained only show a second-order phase transition with a much weaker MCE [80, 90, 91, 93]. However, high purity starting materials increase the production cost, which will limit the broad application of this kind of materials.

Replacing Gd with Tb, it was found that the $Gd_5Si_2Ge_2$-type structure can also be obtained, and a large MCE shows up when the structural transition coincides with the magnetic one, which can be realized by applying a pressure of 8.6 kbar as

shown by Morellon et al. [94]. The maximal entropy change reaches ~22 J/kgK for a field change of 5 T (P=10.2 kbar).

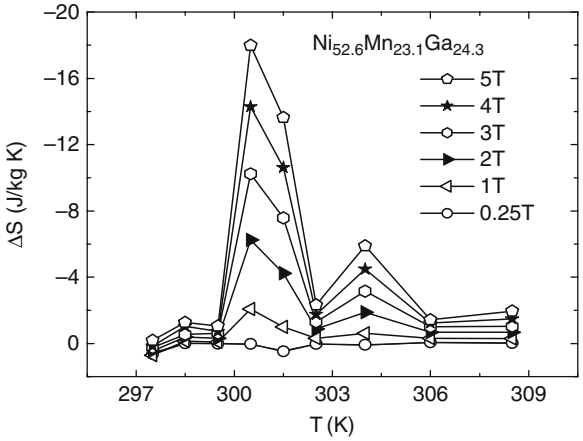

Fig. 15.42 Magnetic entropy change of a single crystal alloy $Ni_{52.6}Mn_{23.1}Ga_{24.3}$ under different magnetic fields (Ref. [97])

15.5.3 Mn-Based Heusler Alloys

The Heusler alloys with the nominal formula of X_2YZ crystallize in the $L2_1$ structure [95]. As shown in Fig. 15.40, the structure is composed of four interpenetrating fcc sublattices, with two of them being occupied by X atoms. In general, the X is a noble or a transition metal, and Z is the atoms with s and p valence electrons. In Mn-based Heusler alloys, Mn occupies the Y sites, and it exhibits a magnetic moment of 4 μ_B if the X sites are not occupied by Co or Fe. As shown by Fig. 15.40, the Mn atom has eight nearest neighboring X and six second neighboring Z. The neighboring Mn atoms appear in the third shell. The typical distance between first, second, and third neighbors are 2.6, 3, and 4.2 Å, respectively. Because of the large distance between Mn atoms, a direct exchange interaction is negligible and the magnetic coupling is mediated by the itinerant electrons of X and Y atoms. Therefore, the magnetic interaction is sensitive to the electronic structure of X and Z. The structural and magnetic properties of the alloys are sensitive to chemical order, compositions, and the lattice parameter. Most of the Mn-based Heusler alloys are FM, such as the typical compound Ni_2MnGa, which is well known for its shape-memory effect, superelasticity, and magnetic-field-induced strain. AFM state appears when the Z sites are occupied by Al or In. Mn carries a magnetic moment of 4 μ_B, while Ni a rather small moment.

Ni−Mn−Ga undergoes a martensitic–austenitic structure transition on heating. Both the martensite and the austenite phases are FM. However, the magnetic behaviors of the two phases are significantly different. The former is hard to be magnetically saturated because of its large magnetocrystalline anisotropy. The

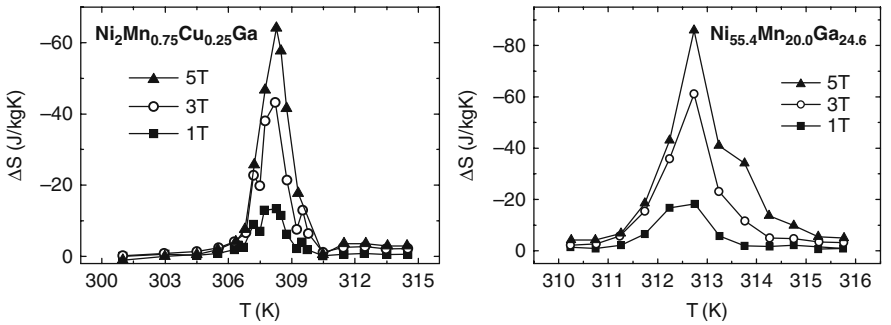

Fig. 15.43 Magnetic entropy change as a function of temperature for a polycrystalline alloys $Ni_2Mn_{0.75}Cu_{0.25}Ga$ (*left*, Ref. [102]) and $Ni_{55.4}Mn_{20.0}Ga_{24.6}$ (*right*, Ref. [103])

simultaneous change of structure and magnetic properties at the phase transition yields significant entropy changes. Since the first report of large ΔS associated with the structure transition in $Ni_{51.5}Mn_{22.7}Ga_{25.8}$ in 2000 (Fig. 15.41) [96], an intensive study on the magnetic and magnetocaloric properties of various Heusler alloys has been stimulated [96,97,98,99,100,101,102,103,104]. It was found that ΔS is positive under low magnetic fields. It becomes negative and increases with applied field when magnetic field is high [98]. As shown in Fig. 15.42, the entropy change of the single crystal $Ni_{52.6}Mn_{23.1}Ga_{24.3}$ is $\sim$18 J/kgK (ΔH=5 T) [97], nearly the same as that of $Gd_5Si_2Ge_2$. The martensitic transition temperature, thus the ΔS peak, can be tuned by the chemical compositions between 150 and 300 K as required. It was recently found an extremely high ΔS can be gained when the structural and magnetic transition coincides with each other. The reported ΔS of -64 J/kgK (ΔH=5 T and T_C=308 K) and -86 J/kgK (ΔH=5 T and T_C=313 K) occurred in polycrystalline $Ni_2Mn_{0.75}Cu_{0.25}Ga$ [102] and single crystal $Ni_{55.4}Mn_{20.0}Ga_{24.6}$[103], respectively (Fig. 15.43). However, there is still no evidence from the thermal data for the giant entropy change at present. The adiabatic temperature change ΔT_{ad} of the Heusler alloys is rarely reported, and the only result is 1.2 K (ΔH=2.6 T), for a polycrystalline alloy $Ni_{54.8}Mn_{20.2}Ga_{25.0}$.

A new kind of Heusler alloys, named meta-magnetic shape-memory alloys (MSMAs), has recently attracted intensive attention [105]. In these materials, the magnetization of martensite phase is very low. Magnetic fields can induce a mantensitic–austenitic transformation, thus a huge shape-memory effect. Meanwhile, the structure transition is accompanied by a significant MCE, and a ΔS spanned in a relatively wide temperature range has been observed [104, 106,107,108]. ΔS is positive, and amounts to $\sim$18 J/kgK (ΔH=5 T and T_C=307 K) for $Ni_{50}Mn_{37}Sn_{13}$ [104] and $\sim$6.8 J/kgK (ΔH=1 T and T_C=307 K) for $Ni_{50}Mn_{39}Sn_{11}$[106] (Fig. 15.44). The wide temperature span (about 5$-$30 K) of ΔS may be the main advantages of MSMAs over the traditional Heusler alloys. The adiabatic temperature change ΔT_{ad} of $Ni_{50}Mn_{34}In_{16}$ is -0.6 K for a field change of 1.3 T [108, 109].

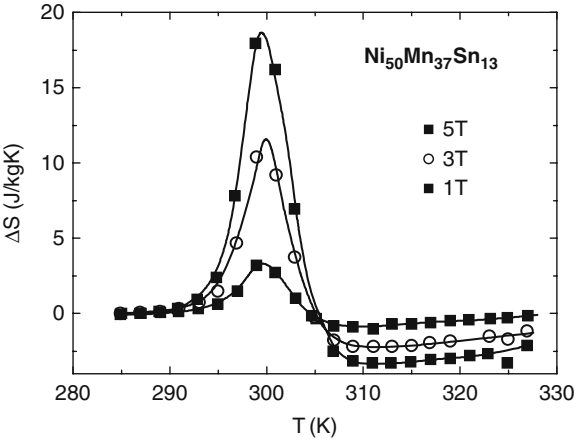

Fig. 15.44 Magnetic entropy change as a function of temperature for a polycrystalline alloy $Ni_{50}Mn_{37}Sn_{13}$ for various changes in applied magnetic field. This figure is reprinted from Ref. [104]

Significant thermal and magnetic hysteresis exists in both the FSMAs and the MSMAs alloys because of the first-order transition. In general, the thermal hysteresis varies between 5 and 20 K, and the magnetic one between 0 and 60 J/kg, crucially depending on compositions. The preparation of Heusler alloys is fairly simple. Polycrystalline samples can be obtained by the arc melting technique. The resulting ingots were homogenized at 1,100 K within 10 days, then quenched into ice water.

15.5.4 Mn−As-Based Compounds

MnAs is a ferromagnet with saturation magnetization of 3.4 μ_B/Mn [110]. A first-order FM−PM transition takes place at $T_C \approx 318$ K. Accompanying this transition, a hexagonal (NiAs-type) to orthorhombic (MnP-type) structure transformation occurs. The resulting MCE is pretty large, and ΔS reaches ∼40 J/kgK and ΔT_{ad} ∼13 K for a field change of 5 T [18, 110]. The MnAs alloy shows large thermal and magnetic hystereses. A substitution of Sb for As can reduce thermal hysteresis and lower T_C to ∼280 K while the MCE effect is not remarkably affected. ΔS still has a value of −30 J/kgK even 10% As was replaced by Sb [18, 110].

$MnFeP_{0.45}As_{0.55}$ is another kind of compounds showing significant MCE [111]. It crystallizes in the hexagonal Fe_2P-type structure, with a Curie temperature of ∼307 K. The magnetic transition is first order with a thermal hysteresis less than 1 K. The maximal ΔS is ∼−18 J/kgK for a field change of 5 T. A variation of the P to As ratio between 3:2 and 1:2 tunes T_C between 200 and 350 K without obviously affecting MCE [112].

The preparation of the $MnAs_{1-x}Sb_x$ and $MnFeP_{1-x}As$ alloys is simple [18, 110,111,112]. However, the high vapor pressure of As and P and the toxicity of As may limit their applications in commercial devices.

15.6 Concluding Remarks

The discovery of giant MCE in $Gd_5Si_2Ge_2$, $LaFe_{13-x}Si_x$, and $MnFeP_{1-x}As_x$, etc. leads the interest of researchers to the material that experience a first-order phase transition, which causes an entropy change concentrated in a narrow temperature range, thus a giant MCE. In addition to the materials discussed here, considerable MCE is also observed in perovskite manganese oxides [113], antiperovskite Mn_3GaC [114], and many other compounds.

In this case, lattice or electronic entropy can also undergo a significant change on the application of magnetic field, therefore is usable for magnetic cooling. These results display a bright prospect of the magnetic refrigeration near ambient temperature.

Compared with other materials, the $LaFe_{13-x}Si_x$ intermetallics show considerable advantages as far as magnetic hysteresis loss, thermal conductive property, and production cost of the materials being concerned. There are also attempts to verify the efficiency of this kind of materials as magnetic refrigerants by putting sphere-shaped $LaFe_{11.18}Si_{1.82}H_\delta$ into an active magnetic regenerator (AMR) test module, and satisfactory result is obtained [115]. However, the existing materials are still far from practical applications. New materials with much stronger MCE are desired to guarantee the high efficiency of the magnetic refrigeration, especially when permanent magnet is used in refrigerators. As far as the practical application being concerned, furthermore, several basic issues involved in the MCE arising from the first-order phase transition must be considered. For example, the effects of magnetic/thermal hysteresis and magnetostriction, the latter may cause a degeneration of the performance of materials because of the mechanical fatigue.

Acknowledgments The authors wish to thank Mrs. Jia Lin for her assistant in preparing part of the figures.

References

1. E. Warburg, Ann. Phys. **13**, 141 (1881).
2. P. Langevin, Ann. Chim. Phy. **5**, 70 (1905).
3. P. Debye, Ann. Phys. **81**, 1154 (1926).
4. W. F. Giauque, J. Amer. Chem. Soc. **49**, 1864 (1927).
5. W. F. Giauque, I. D. P. MacDougall, Phys. Rev. **43**, 768 (1933).
6. P. J. Hakonen, S. Yin, and O. V. Lounasmaa, Phys. Rev. Lett. 64, 2707 (1990).
7. W. F. Giauque, J. Amer. Chem. Soc. **49**, 1864 (1927); W. F. Giauque and D. P. McDougall, Phys. Rev. **43**, 768 (1933).
8. R. D. McMichael, J. J. Ritter, and R. D. Shull, J. Appl. Phys. **73**, 6946 (1993); R. D. Shull and R. D. McMichael, Nanostructure Mater. **2**, 205 (1993); R. D. Shull, IEEE Trans. Magn. **29**, 2614 (1993).
9. T. Hashimoto, T. Kuzuhara, M. Sahashi, K. Inomata, A. Tomokiyo and H. Yayama, J Appl. Phys. **62**, 3873 (1987).
10. T. Hashimoto, T. Kuzuhara, K. Matsumoto, M. Sahashi, K. Imonata, A. Tomokiyo, and H. Yayama, IEEE Trans. Mag. **MAG-23**, 2847 (1987).
11. Tishin A. M. and Y. I. Spichkin, *The magnetocaloric effect and its application*, IOP Publishing Ltd, 2003.

12. G. V. Brown, J. Appl. Phys. **47**, 3673 (1976).
13. C. Zimm, A. Jastrab, A. Sternberg, V. K. Pecharsky, K. Gschneidner Jr, M. Osborne, and I. Anderson, Adv. Cryog. Eng. **43**, 1759 (1998).
14. V. K. Pecharsky and K. A. Gschneidner Jr., Phys. Rev. Lett. **78**, 4494 (1997).
15. V. K. Pecharsky and K. A. Gschneidner Jr., Appl. Phys. Lett. **70**, 3299 (1997).
16. F. X. Hu, B. G. Shen, J. R. Sun, and X. X. Zhang, Chinese Phys. **9**, 550 (2000).
17. F. X. Hu, B. G. Shen, J. R. Sun, and Z. H. Cheng, Appl. Phys. Lett. **78**, 3675 (2001).
18. H. Wada and Y. Tanabe, Appl. Phys. Lett. **79**, 3302 (2001).
19. O. Tegus, E. Brück, K. H. J. Buschow, and F. R. de Boer, Nature **415**, 150 (2002).
20. V. K. Pecharsky and K. A. Gschneidner Jr., J. Appl. Phys. **86**, 565 (1999).
21. J. R. Sun, F. X. Hu, and B. G. Shen, Phys. Rev. Lett. **85**, 4191 (2000).
22. G. J. Liu, J. R. Sun, J. Shen, B. Gao, H. W. Zhang, F. X. Hu, and B. G. Shen, Appl. Phys. Lett. **90**, 032507 (2007).
23. A. de Campos, D. L. Rocco, A. M. G. Carvalho, L. Caron, A. A. Coelho, S. Gama, L. M. da Silva, F. C. G. Gandra, A. D. dos Santos, L. P. Cardoso, P. J. von Rank, and N. A. de Oliveira, Nat. Mater. **5**, 802 (2006).
24. A. Giguère, M. Foldeaki, B. Ravi Gopal, R. Chahine, T. K. Bose, A. Frydman, and J. A. Barclay, Phys. Rev. Lett. **83**, 2262 (1999).
25. S. Gama, A. A. Coelho, A. de Campos, A. Magnus G. Carvalho, and F. C.G. Gandra, Phys. Rev. Lett. **93**, 237202 (2004).
26. A. A. Coelho, S. Gama, F. C. G. Gandra, A. O. dos Santos, L. P. Cardoso, P. J. von Ranke, and N. A. de Oliveira, Appl. Phys. Lett. **90**, 242507 (2007).
27. G. J. Liu, J. R. Sun, J. Z. Wang, and B. G. Shen, Appl. Phys. Lett. **89**, 22503 (2006).
28. V. K. Pecharsky, K. A. Gschneidner Jr., J. Magn. Magn. Mater. **200**, 44 (1999).
29. K. H. J. Buschow, Rep. Progr. Phys. **40**, 1179 (1977).
30. P. I. Kripyakevich, O. S. Zarechnyuk, E. I. Gladushevsky, and O. I. Bodak, Z. Anorg. Chem. **358**, 90 (1968).
31. T. T. M. Palstra, J. A. Mydosh, G. J. Nieuwenhuys, A. M. van der Kraan, and K. H. J. Buschow, J. Magn. Magn. Mater. **36**, 290 (1983).
32. T. T. M. Palstra, G. J. Nieuwenhuys, J. A. Mydosh and K. H. J. Buschow, Phys. Rev. B **31**, 4622 (1985).
33. R. B. Helmholdt, T. T. M. Palstra, G. J. Nieuwenhuys, J. A. Mydosh, A. M. van der Kraan, and K. H. J. Buschow, Phys. Rev. B **34**, 169 (1986).
34. W. H. Tang, J. K. Liang, G. H. Rao, and X. Yan, Phys. Stat. Sol. **141**, 217 (1994).
35. A. Fujita and K. Fukamichi, IEEE. Magb. **35**, 3796 (1999).
36. A. Fujita, Y. Akamatsu, and K. Fukamichi, J. Appl. Phys. **85**, 4756 (1999).
37. F. X. Hu, *Magnetic properties and magnetic entropy change of Fe-based La(Fe,M)$_{13}$ compounds and Ni-Mn-Ga alloys*, Ph. D thesis, Institute of Physics of Chinese academy of Sciences, 2002.
38. L. Jia, J. R. Sun, J. Shen, B. Gao, and B. G. Shen (unpublished).
39. A. Fujita, S. Fujieda, Y. Hasegawa, and K. Fukamichi, Phys. Rev. B **67**, 104416 (2003).
40. G. J. Wang, F. Wang, N. L. Di, B. G. Shen, and Z. H. Cheng, J. Magn. Magn. Mater. **303**, 84 (2006).
41. F. Wang, J. Zhang, Y. F. Chen, G. J. Wang, J. R. Sun, S. Y. Zhang, and B. G. Shen, Phys. Rev. B **69**, 094424 (2004).
42. F. X. Hu, B. G. Shen, J. R. Sun, Z. H. Cheng, and X. X. Zhang, J. Phys.: Condens. Matter **12**, L691 (2000).
43. F. W. Wang, G. J. Wang, F. X. Hu, A. Kurbakov, B. G. Shen, and Z. H. Cheng, J. Phys.: Condens. Matter **15**, 5269(2003).
44. L. Jia, J. R. Sun, H. W. Zhang, F. X. Hu, C. Dong, and B. G. Shen, J. Phys.: Condens. Matter **18**, 9999 (2006).
45. A. Fujita, S. Fujieda, K. Fukamichi, Y. Yamazaki, Y. Iijima, Mater. Trans. **43**, 1202 (2002).
46. S. Fujieda, A. Fujita, and K. Fukamichi, Appl. Phys. Lett. **81**, 1276 (2002).

47. F. X. Hu, J. Gao, X. L. Qian, M. Ilyn, A. M. Tishin, J. R. Sun, and B. G. Shen, J. Appl. Phys. **97**, 10M303 (2005).
48. M. Balli, D. Fruchart, and D. Gignoux, J. Phys.: Condens. Matter **19**, 236230 (2007).
49. F. Wang, J. Zhang, Y. F. Chen, G. J. Wang, J. R. Sun, S. Y. Zhang, and B. G. Shen, Phys. Rev. B **69**, 094424 (2004).
50. S. Fujieda, A. Fujita, N. Kawamoto, and K. Fukamichi, Appl. Phys. Lett. **89**, 062504 (2006).
51. D. T. Kim Anh, N. P. Thuy a,b, N. H. Duca, T. T. Nhiena, and N. V. Nong, J. Magn. Magn. Mater. **262**, 427 (2003).
52. S. Fujieda, A. Fujita, and K. Fukamichi, Mater. Trans. **45**, 3228 (2004).
53. S. Fujieda, A. Fujita, and K. Fukamichi, IEEE Trans. Magn. **41**, 2787 (2005).
54. S. Fujieda, A. Fujita, K. Fukamichi, N. Hirano, and S. Nagaya, J. Alloys. Comp. **408–412**, 1165 (2006).
55. S. Fujieda, A. Fujita, N. Kawamoto, and K. Fukamichi, J. Appl. Phys. **99**, 08K910 (2006).
56. A. Fujita, S. Fujieda, and K. Fukamichi, J. Magn. Magn. Mater. **310**, E1006–E1007 (2007).
57. J. Shen, Y. X. Li, B. Gao, F. X. Hu, J. R. Sun, and B. G. Shen (unpublished).
58. J. Shen, B. Gao, L. Q. Yan, Y. X. Li, H. W. Zhang, F. X. Hu, and J. R. Sun, Chinese Phys. **16**, 3848 (2007).
59. S. Fujieda, A. Fujita, and K. Fukamichi, J. Magn. Magn. Mater. **310**, e1004 (2007).
60. S. Fujieda, A. Fujita, and K. Fukamichi, J. Appl. Phys. **102**, 023907 (2007).
61. Sun et al. unpublished.
62. S. Fujieda, A. Fujita, K. Fukamichi, Y. Yamazaki, and Y. Iijima, Appl. Phys. Lett. **79**, 653 (2001).
63. A. Fujita, S. Fujieda, K. Fukamichi, Y. Yamazaki, and Y. Iijima, Mater. Trans. **43**, 1202–1204 (2002).
64. A. Fujita, S. Fujieda, Y. Hasegawa, and K. Fukamichi, Phys. Rev. B **67**, 104416 (2003).
65. Y. F. Chen, F. Wang, B. G. Shen, F. X. Hu, Z. H. Cheng, G. J. Wang, and J. R. Sun, Chin. Phys. **11**, 741 (2002).
66. Y. F. Chen, F. Wang, B. G. Shen, F. X. Hu, J. R. Sun, G. J. Wang, and Z. H. Cheng, J. Phys.: Condens. Matter **15**, L161–L167 (2003).
67. Z. X. Tang, X. H. Deng, G. C. Hadjipanayis, V. Papaefthymiou and D. J. Sellmyer, IEEE Trans. Magn. **29**, 2839 (1993).
68. J. P. Liu, N. Tang, F. R. de Boer, P. F. de Chatel, and K. H. J. Buschow, J. Magn. Magn. Mater. **140–144**, 1035 (1995).
69. O. Moze, W. Kockelmann, J. P. Liu, F. R. de Boer, and K. H. J. Buschow, J. Magn. Magn. Mater. **195**, 391 (1999).
70. O. Moze, W. Kockelmann, J. P. Liu, F. R. de Boer, and K. H. J. Buschow, J. Appl. Phys. **87**, 5284 (2000).
71. K. Irisawa, A. Fujita, K. Fukamichi, Y. Yamazaki, Y. Iijima, and E. Matsubara, J. Alloys Comp. **316**, 70 (2001).
72. S. Fujieda, A. Fujita, K. Fukamichi, Y. Yamazaki, and Y. Iijima, Appl. Phys. Lett. **79**, 653 (2001).
73. K. Fukamichi, A. Fujita, and S. Fujieda, J. Alloys Comp. **408–412**, 307 (2006).
74. S. Fujieda, A. Fujita, and K. Fukamichi, J. Appl. Phys. **102**, 023907 (2007).
75. F. Wang, *Magnetic and magnetocaloric properties of* $NaZn_{13}$-type $La(Fe,M)_{13}$ intermetallics, *Ph.D. thesis, Institute of Physics of Chinese Academy of Sciences*, 2004.
76. Y. F. Chen, F. Wang, B. G. Shen, F. X. Hu, J. R. Sun, G. J. Wang, and Z. H. Cheng, J. Appl. Phys. **93**, 1323 (2003).
77. L. Jia, J. R. Sun, J. Shen, B. Gao, T. Y. Zhao, H. W. Zhang, F. X. Hu, and B. G. Shen (unpublished).
78. J. Shen, B. Gao, H. W. Zhang, F. X. Hu, Y. X. Li, J. R. Sun, and B. G. Shen, Appl. Phys. Lett. **91**, 142504 (2007).
79. X. X. Zhang, G. H. Wen, F. W. Wang, W. H. Wang, C. H. Yu, and G. H. Wu, Appl. Phys. Lett. **77**, 3072 (2000).

80. A. O. Pecharsky, K. A. Gschneidner Jr., V. K. Pecharsky, and C. E. Schindler, J. Alloys Comp. **338**, 126 (2002).
81. V. K. Pecharsky, A. O. Pecharsky, and K. A. Gschneidner Jr., J. Alloys Comp. **344**, 362 (2002).
82. A. O. Pecharsky, K. A. Gschneidner Jr., and V. K. Pecharsky, J. Magn. Magn. Mater. **267**, 60 (2003).
83. Y. Zhuo, R. Chahine, and T. K. Bose, IEEE Trans. Magn. **39**, 3358 (2003).
84. A. Giguìere, M. Foldeaki, B. R. Gopal, R. Chahine, T. K. Bose, A. Frydman, and J. A. Barclay, Phys. Rev. Lett. **83**, 2262 (1999).
85. K. A. Gschneidner Jr., V. K. Pecharsky, E. Brück, H. G. M. Duijn, and E. M. Levin, Phys. Rev. Lett. **85**, 4190 (2000).
86. K. A. Gschneidner Jr., V. K. Pecharsky, and A. O. Tsokoll, Rep. Prog. Phys. **68**, 1479 (2005).
87. F. Holtzberg, R. J. Gambino, T. R. McGuire, J. Phys. Chem. Solids, **28**, 2283 (1967).
88. A. O. Pecharsky, K. A. Gschneidner Jr., and V. K. Pecharsky, J. Appl. Phys. **93**, 4722 (2003).
89. V. K. Pecharsky and K. A. Gschneidner Jr., J. Magn. Magn. Mater. **167**, L179 (1997).
90. E. M. Levina, K. A. Gschneidner Jr., and V. K. Pecharsky, J. Magn. Magn. Mater. **231** (2001) 135.
91. O. Tegus, E. Bruck, L. Zhang, Dagula, K. H. J. Buschow, and F. R. de Boer, Physica B **319** (2002) 174.
92. H. Tang, A. O. Pecharsky, D. L. Schlagel, T. A. Lograsso, V. K. Pecharsky, and K. A. Gschneidner Jr., J. Appl. Phys. **93**, 8298 (2003).
93. V. Provenzano, A. J. Shapiro, and R. D. Shull, Nature **429**, 853 (2004).
94. L. Morellon, Z. Arnold, C. Magen, C. Ritter, O. Prokhnenko, Y. Skorokhod, P. A. Algarabel, M. R. Ibarra, and J. Kamarad, Phys. Rev. Lett. **93**, 137201 (2004).
95. P. J. Webster, Contemp. Phys. **10**, 559 (1969).
96. F. X. Hu, B. G. Shen, and J. R. Sun, Appl. Phys. Lett. **76**, 3460 (2000).
97. F. X. Hu, B. G. Shen, J. R. Sun, and G. H. Wu, Phys. Rev. B **64**, 132412 (2001).
98. F. X. Hu, J. R. Sun, G. H. Wu, and B. G. Shen, J. Appl. Phys. **90**, 5216 (2001).
99. J. Marcos, L. Mañosa, A. Planes, F. Casanova, X. Batlle, and A. Labarta, Phys. Rev. B **68**, 094401 (2003).
100. F. Albertini, F. Canepa, S. Cirafici, E. A. Franceschi, M. Napoletano, A. Paoluzi, L. Pareti, and M. Solzi, J. Magn. Magn. Mater. **272–276**, 2111 (2004).
101. X. Zhou, W. Li, H. P. Kunkel, and G. Williams, J. Phys.: Condens. Matter **16**, L39 (2004).
102. S. Stadler, M. Khan, J. Mitchell, N. Ali, A. M. Gomes, I. Dubenko, A. Y. Takeuchi, and A. P. Guimarães, Appl. Phys. Lett. **88**, 192511 (2006).
103. M. Pasquale, C. P. Sasso, L. H. Lewis, L. Giudici, T. Lograsso, and D. Schlagel, Phys. Rev. B **72**, 094435 (2005).
104. T. Krenke, E. Duman, M. Acet, E. F. Wassermann, X. Moya, L. Mañosa, and A. Planes, Nat. Mater. **4**, 450 (2005).
105. R. Kainuma, Y. Imano, W. Ito, Y. Sutou, H. Morito, S. Okamoto, O. Kitakami, K. Oikawa, A. Fujita, T. Kanomata, and K. Ishida, Nature **439**, 957 (2006).
106. Z. D. Han, D. H. Wang, C. L. Zhang, H. C. Xuan, B. X. Gu, and Y. W. Du, Appl. Phys. Lett. **90**, 042507 (2007).
107. T. Krenke, E. Duman, M. Acet, and E. F. Wassermann, X. Moya, L. Mañosa, A. Planes, E. Suard, and Bachir Ouladdiaf, Phys. Rev. B **75**, 104414 (2007).
108. X. Moya, L. Mañosa, A. Planes, S. Aksoy, M. Acet, E. F. Wassermann, and T. Krenke, Phys. Rev. B **75**, 184412 (2007).
109. C. Guillaud, J. Phys. Radium **12**, 223 (1951).
110. H. Wada, T. Morikawaa, K. Taniguchia, T. Shibatab, Y. Yamadab, and Y. Akishige, Physica B **328**, 114 (2003).
111. O. Tegus, E. Brück, K. H. J. Buschow, and F. R. de Boer, Nature **415**, 150 (2002).
112. O. Tegus, E. Brück, L. Zhang, Dagula, K. H. J. Buschow, and F. R. de Boer, Physica B **319**, 174 (2002).

113. M.-H. Phana and S.-C. Yub, J. Magn. Magn. Mater. **308**, 325 (2007).
114. T. Tohei, H. Wada, and T. Kanomata, J. Appl. Phys. **94**, 1800 (2003).
115. A. Fujita, S. Koiwai, S. Fujieda, K. Fukamichi, T. Kobayashi, H. Tsuji, S. Kaji, and A. T. Saito, Jpn. J. Appl. Phys. Pt. 2, **46**, L154 (2007).